Zero-Field Splitting Parameters within Exact Two-Component Theory and Modern Density Functional Theory Using Seminumerical Integration

Florian Bruder,[1] Yannick J. Franzke*,[1] Christof Holzer,[2] and Florian Weigend*[1]
[1] *Fachbereich Chemie, Philipps-Universität Marburg, Hans-Meerwein-Straße 4, 35032 Marburg, Germany*
[2] *Institute of Theoretical Solid State Physics, Karlsruhe Institute of Technology (KIT), Wolfgang-Gaede-Straße 1, 76131 Karlsruhe, Germany*

(*Email for correspondence: florian.weigend@chemie.uni-marburg.de)

(*Email for correspondence: yannick.franzke@chemie.uni-marburg.de)

(Dated: 6 September 2023)

An efficient implementation of zero-field splitting parameters based on the work of Schmitt *et al.* [*J. Chem. Phys.* **134**, 194113 (2011)] is presented. Seminumerical integration techniques are used for the two-electron spin–dipole contribution and the response equations of the spin–orbit perturbation. The original formulation is further generalized. First, it is extended to meta-generalized gradient approximations (meta-GGAs) and local hybrid functionals. For these functional classes, the response of the paramagnetic current density is considered in the coupled-perturbed Kohn–Sham (CPKS) equations for the spin–orbit perturbation term. Second, the spin–orbit perturbation is formulated within the relativistic exact two-component (X2C) theory and the screened nuclear spin–orbit (SNSO) approximation. Accuracy of the implementation is demonstrated for transition-metal and diatomic main-group compounds. The efficiency is assessed for Mn and Mo complexes. Here, it is found that coarse integration grids for the seminumerical schemes lead to drastic speedups while introducing clearly negligible errors. Additionally, the SNSO approximation substantially reduces the computational demands and leads to very similar results as the spin–orbit mean field (SOMF) ansatz.

I. INTRODUCTION

Zero-field splitting (ZFS) plays a crucial role in the characterization of magnetic systems. Various quantum-chemical descriptions of this property have therefore been established within the framework of density functional theory[1–12] (DFT) or wavefunction-based (multi-reference) methods.[13–24] In addition to its importance in describing magnetic systems, the ZFS is also of great relevance for the temperature-dependent contribution of paramagnetic nuclear magnetic resonance (pNMR) spectra with more than one unpaired electron.[25–28] The ZFS tensor $\boldsymbol{D}$ is generally split into the spin–dipolar (SD) and spin–orbit (SO) terms. The form of the SD contribution is generally agreed upon, see for example refs. 9,29–31. Two important developments for the SD contribution were presented by the Neese group. The first was the suggestion to compute the spin-excess density matrix for the SD term based on unrestricted natural orbitals[32] (UNOs) to avoid spin-contamination.[3] Second, the resolution of the identity (RI) approximation was introduced to reduce the computational effort for the SD term.[20]

In contrast to the SD term, two different routes were taken towards the calculation of the SO contribution in the past. The first one makes use of the relationship between $\boldsymbol{D}$ and the magnetic anisotropy energy. A DFT-based approach relying on the magnetic anisotropy energy was first presented by Pederson and Khanna[1] (PK approach) and considers spin–orbit coupling within second-order perturbation theory, without a formal consideration of exact or Hartree–Fock (HF) exchange. The second approach starts at a sum-over-states formulation for the $\boldsymbol{D}$ tensor, as originally outlined by Neese and Solomon.[13] This approach is conceptually closer to a wavefunction-based approach, and was subsequently applied within the DFT framework by Neese and labelled as "quasi-restricted orbital" (QRO) method.[4] In a follow-up work, the sum-over-states approach was reformulated using a derivative-based ansatz, resulting in a coupled-perturbed Kohn–Sham (CPKS) formalism called "CP-SOC", which also formally accounts for exact exchange.[5] Investigating the relationship between the magnetic anisotropy energy and the $\boldsymbol{D}$ tensor,[8] the group of van Wüllen proposed a different treatment of the spin within the PK approach, resulting in revised prefactors.[9] Additionally, a set of CPKS equations was presented including exact exchange. By pointing out an error in the derivation starting from the sum-over-states formalism, it was demonstrated that the two routes towards the SO contribution of the $\boldsymbol{D}$ tensor lead to the same result.[9]

In this work, we aim at improving the quality and computational accessibility of ZFS parameters in three distinct ways. First, seminumerical integration techniques[33–43] will be applied. This allows for an efficient yet accurate evaluation of the two-electron spin–dipole integrals. Second, the classes of meta-GGAs and local hybrid functionals[44] (LHFs) will be made available for calculating ZFS. This necessitates the incorporation of the paramagnetic current density to set up the generalized kinetic-energy density.[45–56] As shown previously,[49–54] this is of particular relevance for magnetic properties with the Minnesota functionals[57,58] and also generally improves the results with the SCAN functional family.[59–62] Third, the exact two-component (X2C) approach[63–69] and the relativistic picture-change correction will be applied to the spin–orbit perturbation. As molecular systems containing heavy elements require a consideration of both scalar-relativistic and spin–orbit effects, this is expected to considerably improve the *in silico* prediction of the related parameters.[70–79]

II. THEORY

The zero-field splitting Hamiltonian for a single effective spin is given by

$$\hat{H}^{\mathrm{ZFS}} = \hat{\vec{S}}\boldsymbol{D}\hat{\vec{S}}, \tag{1}$$

where $\hat{\vec{S}}$ is the effective spin-operator and $\boldsymbol{D}$ is the ZFS tensor. From the components of the full ZFS tensor $\boldsymbol{D}$, the axial ZFS parameter D, the rhombic parameter E, and the rhombicity parameter E/D can be defined using the elements of the diagonalized tensor by

$$\begin{aligned} \mathrm{D} &= D_{zz} - \frac{1}{2}\left(D_{xx} + D_{yy}\right), && (2)\\ \mathrm{E} &= \frac{1}{2}\left(D_{xx} - D_{yy}\right), && (3)\\ 0 &\leq \mathrm{E/D} \leq 1/3. && (4) \end{aligned}$$

The last condition is often used to arrive at a standardized way of expressing these parameters.[29] The parameters D and E characterize the energy splitting of the sublevels within a spin multiplet and are important quantities in the framework of electron paramagnetic resonance (EPR) spectroscopy.[80–83] In a coordinate system which diagonalizes the ZFS tensor, the Hamiltonian can be rewritten with help of the ZFS parameters D and E according to

$$\hat{H}^{\mathrm{ZFS}} = \mathrm{D}\left[\hat{S}_z^2 - \frac{1}{3}S(S+1)\right] + \mathrm{E}\left[\hat{S}_x^2 - \hat{S}_y^2\right], \tag{5}$$

where S is the total effective spin, see ref. 29 for details. A non-vanishing ZFS tensor is a prerequisite for the occurrence of magnetic anisotropy, which describes the dependence of the ground-state energy on the direction $\vec{n}$ of the magnetic field. If the spin is aligned along $\vec{n}$ and if $\boldsymbol{D}$ is traceless, the magnetic anisotropy energy can be calculated by[8,9]

$$W(\vec{n}) = S\left(S - \frac{1}{2}\right)\vec{n}\cdot\boldsymbol{D}\cdot\vec{n}, \tag{6}$$

which is straightforwardly accessible only by two or four-component ground-state calculations. In the one-component case, the spin is generally aligned along the z axis.

A. Two-Electron Spin–Dipole Term

The spin-dipolar (SD) contribution[30,31] to the ZFS tensor reads

$$\begin{aligned} D_{pq}^{\mathrm{SD}} =& \frac{1}{S(S-1/2)}\frac{1}{8c^2}\sum_{\mu,\nu,\kappa,\lambda}\left(P_{\mu\nu}^{\mathrm{S}}P_{\kappa\lambda}^{\mathrm{S}} - P_{\mu\lambda}^{\mathrm{S}}P_{\kappa\nu}^{\mathrm{S}}\right)\times \\ & \langle\mu(\vec{r}_1)\kappa(\vec{r}_2)|\frac{\delta_{pq}}{r_{12}^3} - \frac{3p_{12}q_{12}}{r_{12}^5}|\nu(\vec{r}_1)\lambda(\vec{r}_2)\rangle\,. \end{aligned} \tag{7}$$

Here, we have explicitly listed the coordinate for all (real-valued) basis functions $(\chi_\mu, \chi_\nu, \chi_\kappa, \chi_\lambda)$. r denotes the norm of the position vector, i.e. $r_{12} = |\vec{r}_1 - \vec{r}_2|$, and p, q are the respective Cartesian vector components. Note that the SD term is evaluated with 100% of exact exchange ($a_{\mathrm{X}} = 1$) and 0% semilocal DFT contribution.[9] $P_{\mu\nu}^{\mathrm{S}}$ is a matrix element of the spin-excess density matrix,

$$\begin{aligned} P_{\mu\nu}^{\mathrm{S}} &= P_{\mu\nu}^{\alpha} - P_{\mu\nu}^{\beta}, && (8)\\ P_{\mu\nu}^{\sigma} &= \sum_i n_i^{\sigma} c_{\mu i}^{*\sigma} c_{\nu i}^{\sigma}, && (9) \end{aligned}$$

with the coefficients $c_{\mu i}^{\sigma}$ $(\sigma = \alpha, \beta)$ for the spin orbital i. In a standard one-component formalism, these are real-valued and the complex conjugate is therefore trivial. Here, the spin-excess density matrix $\mathbf{P}^{\mathrm{S}}$ can be constructed directly from the canonical coefficients or from natural orbitals.[3] For brevity, we define the four-center two-electron integrals as

$$(\mu\nu|\kappa\lambda)_{pq}^{\mathrm{SD}} = \langle\mu(\vec{r}_1)\kappa(\vec{r}_2)|\frac{\delta_{pq}}{r_{12}^3} - \frac{3p_{12}q_{12}}{r_{12}^5}|\nu(\vec{r}_1)\lambda(\vec{r}_2)\rangle\,. \tag{10}$$

Thus, we may now write the SD term in the form

$$D_{pq}^{\mathrm{SD}} = \frac{1}{S(S-1/2)}\frac{1}{8c^2}\sum_{\mu,\nu}P_{\mu\nu}^{\mathrm{S}}\left[J_{\mu\nu,pq}^{\mathrm{SD}} - K_{\mu\nu,pq}^{\mathrm{SD}}\right] \tag{11}$$

with the Coulomb and exchange matrices

$$\begin{aligned} J_{\mu\nu,pq}^{\mathrm{SD}} &= \sum_{\kappa,\lambda}P_{\kappa\lambda}^{\mathrm{S}}(\mu\nu|\kappa\lambda)_{pq}^{\mathrm{SD}}, && (12)\\ K_{\mu\nu,pq}^{\mathrm{SD}} &= \sum_{\kappa,\lambda}P_{\kappa\lambda}^{\mathrm{S}}(\mu\lambda|\kappa\nu)_{pq}^{\mathrm{SD}}. && (13) \end{aligned}$$

For reasons of economy and in order to avoid the effort to explicitly implement new two-electron integrals, we evaluate the SD term seminumerically in a similar fashion as the Coulomb and exchange integrals for the self-consistent field (SCF) procedure.[33–43] That is, we carry out one integration analytically and the other numerically on a grid. Thus, the integrals over $\vec{r}_1$ are evaluated analytically at given grid points $\vec{r}_g$ to yield

$$A_{\mu\nu,pq}^{\mathrm{SD}}(\vec{r}_g) = \int \chi_\mu(\vec{r}_1)\left[\frac{\delta_{pq}}{r_{1g}^3} - \frac{3p_{1g}q_{1g}}{r_{1g}^5}\right]\chi_\nu(\vec{r}_1)\,d\vec{r}_1 \tag{14}$$

with $r_{1g} = |\vec{r}_1 - \vec{r}_g|$ and the four-center two-electron integrals $(\mu\nu|\kappa\lambda)^{\mathrm{SD}}$ are approximated by

$$\begin{aligned} (\mu\nu|\kappa\lambda)_{pq}^{\mathrm{SD,sn}} =& \frac{1}{2}\sum_g^{n_g} w_g A_{\mu\nu,pq}^{\mathrm{SD}}(\vec{r}_g)\chi_\kappa(\vec{r}_g)\chi_\lambda(\vec{r}_g) \\ &+ \frac{1}{2}\sum_g^{n_g} w_g \chi_\mu(\vec{r}_g)\chi_\nu(\vec{r}_g)A_{\kappa\lambda,pq}^{\mathrm{SD}}(\vec{r}_g) \end{aligned} \tag{15}$$

with the integration weights w_g and n_g grid points. Note that we have chosen a symmetric form for the application of the seminumerical scheme. For a finite grid, the first and the second term may yield different contributions and lead to so-called locality errors. These can be corrected with dealiasing procedures. Details on the screening procedure and suitable dealiasing schemes for high accuracy are discussed in ref. 41.

After application of the seminumerical integration, the Coulomb and exchange contributions are given by

$$J_{\mu\nu}^{\mathrm{SD,sn},+} = \sum_{\kappa,\lambda} (\mu\nu|\kappa\lambda)_{pq}^{\mathrm{SD,sn}} \, P_{\kappa\lambda}^{\mathrm{S},+}, \tag{16}$$

$$K_{\mu\nu}^{\mathrm{SD,sn},+} = \frac{1}{2}\left[\sum_{\kappa,\lambda} (\mu\lambda|\nu\kappa)_{pq}^{\mathrm{SD,sn}} + (\mu\kappa|\nu\lambda)_{pq}^{\mathrm{SD,sn}}\right] P_{\kappa\lambda}^{\mathrm{S},+}, \tag{17}$$

$$K_{\mu\nu}^{\mathrm{SD,sn},-} = \frac{1}{2}\left[\sum_{\kappa,\lambda} (\mu\lambda|\nu\kappa)_{pq}^{\mathrm{SD,sn}} - (\mu\kappa|\nu\lambda)_{pq}^{\mathrm{SD,sn}}\right] P_{\kappa\lambda}^{\mathrm{S},-}. \tag{18}$$

For completeness, we listed both the symmetric (+) and antisymmetric (−) linear combinations of the exchange part. Note that we only consider the symmetric linear combination for the SD exchange part in the following, as the ground-state density matrix $\mathbf{P}^{\mathrm{S}}$ is symmetric, i.e. $\mathbf{P}^{\mathrm{S},-}$ vanishes, and we drop the superscript + for brevity. In contrast, the antisymmetric linear combination of the seminumerical framework is needed for the exchange integrals in the CPKS equations for the spin–orbit perturbation terms in the following section. Defining the shorthand notations $X_\mu^g = \chi_\mu(\vec{r}_g)$ and $A_{\kappa\lambda,pq}^{\mathrm{SD}}(\vec{r}_g) = A_{\kappa\lambda,pq}^{\mathrm{SD},g}$, the Coulomb part of the SD term finally reads

$$J_{\mu\nu}^{\mathrm{SD,sn}} = \frac{1}{2}\sum_{g}^{n_g} w_g \sum_{\kappa\lambda} \left[A_{\mu\nu,pq}^{\mathrm{SD},g} X_\kappa^g X_\lambda^g + X_\mu^g X_\nu^g A_{\kappa\lambda,pq}^{\mathrm{SD},g}\right] P_{\kappa\lambda}^{\mathrm{S}} \tag{19}$$

and the exchange contribution follows as

$$K_{\mu\nu,pq}^{\mathrm{SD,sn}} = \frac{1}{2}\sum_{g}^{n_g} w_g \sum_{\kappa\lambda} \left[X_\mu^g X_\kappa^g A_{\nu\lambda,pq}^{\mathrm{SD},g} + A_{\nu\kappa,pq}^{\mathrm{SD},g} X_\mu^g X_\lambda^g\right] P_{\kappa\lambda}^{\mathrm{S}}. \tag{20}$$

Here, the symmetries of real orbitals were again exploited for the exchange part, e.g. $A_{\mu\nu}^{\mathrm{SD},g} = A_{\nu\mu}^{\mathrm{SD},g}$ and $\sum_\mu X_\mu^g P_{\mu\nu} = \sum_\nu X_\nu^g P_{\mu\nu}$. This reduces the number of terms from four to two for the exchange part. Compared to the pseudospectral or seminumerical schemes for SCF energies,[33–43] only the one-electron SD integrals are used for the matrix A instead of the electrostatic integrals

$$A_{\mu\nu}(\vec{r}_g) = \int \frac{\chi_\mu(\vec{r}_1)\chi_\nu(\vec{r}_1)}{r_{1g}} \, d\vec{r}_1. \tag{21}$$

Thus, the implementation of the SD term based on an existing seminumerical implementation is almost trivial and straightforward. Note that this strategy is not restricted to the two-electron SD term.

B. Same-Spin Spin–Orbit Perturbation

Following the derivations of Schmitt *et al.* in ref. 9, the spin-orbit (SO) contribution to the ZFS tensor can be divided into the same-spin and the spin-flip contributions. These are evaluated with response equations starting from a spin–orbit perturbation term. The same-spin contributions for spin σ are given by

$$D_{pq}^{\mathrm{SO},\sigma} = \frac{1}{S(S-1/2)} \sum_{\mu,\nu} h_{\mu\nu}^{\mathrm{SO},p} \sum_{i,a} c_{\mu i}^{*\sigma} c_{\nu a}^{\sigma} O_{ai}^{\sigma,q}, \tag{22}$$

where i denotes occupied, a unoccupied spin orbitals and $O_{ai}^{\sigma,q}$ is the same-spin orbital rotation matrix of the CPKS equations with respect to the spin–orbit perturbation in q direction according to

$$O_{ai}^{\sigma,q} = \frac{F_{ai}^{\sigma,q}}{\varepsilon_i^\sigma - \varepsilon_a^\sigma}. \tag{23}$$

Here, $F_{ai}^{\sigma,q}$ is the Fock matrix perturbed by the qth component of the spin–orbit coupling Hamiltonian, $h_{\mu\nu}^{\mathrm{SO},p}$. Different spin–orbit Hamiltonians can be chosen as described in the appendix A. Note that the prefactor of $1/4$ is not explicitly shown as in ref. 9. See the definition of $h_{\mu\nu}^{\mathrm{SO},p}$ in the appendix. Additionally, $h_{\mu\nu}^{\mathrm{SO},p}$ is purely imaginary and antisymmetric. For the local spin density approximation (LSDA) and the generalized-gradient approximation (GGA), the contributions from the exchange-correlation (XC) kernel in the CPKS equations vanish due to symmetry reasons for a purely imaginary and antisymmetric perturbation.[84] In other words, the SO perturbation does not cause a response of the electron density and the CPKS formalism is very similar to NMR shifts.[84,85] Thus, the CPKS equations only include the spin–orbit perturbation and the exchange contribution, as the Coulomb part also vanishes.

For the integral evaluation of the CPKS equations, it is convenient to construct the perturbed density matrix explicitly. The orbital rotation matrix can be used to construct the purely imaginary and antisymmetric response density matrix $P_{\mu\nu}^{\sigma,q}$ via

$$c_{\mu i}^{\sigma,q} = \sum_a c_{\mu a}^{\sigma} O_{ai}^{\sigma,q}, \tag{24}$$

$$P_{\mu\nu}^{\sigma,q} = \sum_i \left[n_i^\sigma c_{\mu i}^{*\sigma} c_{\nu i}^{\sigma,q} + n_i^\sigma c_{\mu i}^{*\sigma,q} c_{\nu i}^{\sigma}\right]. \tag{25}$$

Note that the unperturbed coefficients are purely real, while the perturbed coefficients are purely imaginary. Application of the seminumerical scheme for the CPKS part is straightforward. For a purely imaginary and antisymmetric density matrix, the seminumerical exchange (snK) for the CPKS equations can be written as

$$K_{\mu\nu}^{\sigma,q} = \frac{a_{\mathrm{X}}}{2}\sum_g w_g \sum_{\kappa\lambda} \left[X_\mu^g X_\kappa^g A_{\nu\lambda}^g - A_{\nu\kappa}^g X_\mu^g X_\lambda^g\right] P_{\kappa\lambda}^{\sigma,q} \tag{26}$$

with a_{X} denoting the amount of exact exchange for global hybrid density functional approximations.

The CPKS procedure becomes more involved for meta-GGAs. The application of meta-GGAs requires to consider the kinetic-energy density

$$\tau^\sigma = \frac{1}{2}\sum_i |\hat{\vec{p}}\,\varphi_i^\sigma|^2 = \frac{1}{2}\sum_i \left(\hat{\vec{p}}\varphi_i^\sigma\right)^\dagger \cdot \left(\hat{\vec{p}}\varphi_i^\sigma\right) \tag{27}$$

with the Kohn–Sham (spin) orbitals φ_i^σ. Similar to magnetic fields and moments, the spin–orbit perturbation induces a current density and thus current-carrying states are obtained in the response equations. This means that the quantity τ does no longer ensure the proper iso-orbital constraint.[48] Therefore, the kinetic-energy density needs to be generalized to[45–47]

$$\tilde{\tau}^\sigma = \tau^\sigma - \frac{|\vec{j}_p^\sigma|^2}{2\rho^\sigma} \tag{28}$$

which includes the electron (spin) density ρ^σ and the paramagnetic current density[86]

$$\vec{j}_p^\sigma = -\frac{\mathrm{i}}{2}\sum_i \left(\varphi_i^{\sigma,*}\vec{\nabla}\varphi_i^\sigma - \varphi_i^\sigma\vec{\nabla}\varphi_i^{\sigma,*}\right) = \mathrm{Re}\sum_i \left(\varphi_i^{\sigma,*}\ \hat{\vec{p}}\ \varphi_i^\sigma\right). \tag{29}$$

Note that τ is a symmetric quantity, while $\vec{j}_p$ is antisymmetric, i.e. they are evaluated from a symmetric $(+)$ or antisymmetric $(-)$ density matrix

$$\tau^\sigma(\vec{r}) = \frac{1}{2}\sum_{\mu,\nu} P_{\mu\nu}^{\sigma,+}\left[\vec{\nabla}\chi_\mu(\vec{r})\cdot\vec{\nabla}\chi_\nu(\vec{r})\right], \tag{30}$$

$$\vec{j}_\mathrm{p}^\sigma(\vec{r}) = -\frac{\mathrm{i}}{2}\sum_{\mu,\nu} P_{\mu\nu}^{\sigma,-}\left[\vec{\nabla}\chi_\mu(\vec{r})\chi_\nu(\vec{r}) - \chi_\mu(\vec{r})\vec{\nabla}\chi_\nu(\vec{r})\right] \tag{31}$$

Thus, the paramagnetic current density vanishes for the nonrelativistic or scalar-relativistic ground-state SCF calculation and only τ needs to be evaluated. However, the situation is reversed for the CPKS part. Here, the current density does not vanish for the perturbation. This leads to the so-called magnetic XC kernel for the left-hand side of the CPKS equations and requires to evaluate

$$\frac{\delta^2 E_\mathrm{slXC}}{\delta j_{\mathrm{p},u}(\vec{r})\ \delta j_{\mathrm{p},v}(\vec{r}')} = -\frac{\delta_{uv}}{\rho}\left(\frac{\partial f}{\partial\tilde{\tau}}\right)\delta\left(\vec{r}-\vec{r}'\right) \tag{32}$$

where f describes the specific functional form and E_slXC the semilocal exchange-correlation energy. In practice, this also requires to explicitly compute the response of the paramagnetic current density, see ref. 48 for details. Finally, inclusion of the current density means that meta-GGAs always necessitate an iterative solution of the CPKS equations, even for pure semilocal functionals.

Local hybrid functionals allow for a fully position-dependent admixture of exact exchange according to

$$E_\mathrm{XC}^\mathrm{LHF} = \sum_\sigma \int \left[\{1-g(\vec{r})\}\, e_{\mathrm{X},\sigma}^\mathrm{sl}(\vec{r}) + g(\vec{r})e_{\mathrm{X},\sigma}^\mathrm{HF}(\vec{r})\right] d\vec{r} + E_\mathrm{C} \tag{33}$$

with the semilocal DFT exchange energy density $e_{\mathrm{X},\sigma}^\mathrm{sl}$, the exact exchange or HF exchange density $e_{\mathrm{X},\sigma}^\mathrm{HF}$, and the semilocal correlation energy E_C. Just like for global hybrids, the correlation contribution is of the same form as for pure semilocal density functional approximations. $g(\vec{r})$ is a so-called local mixing function (LMF), which controls the admixture of exact exchange. The most widely used LMF is based on the iso-orbital indicator[44] (t-LMF) but also other approaches based on the correlation length (z-LMF) and related quantities were suggested.[87,88] See also ref. 89 for an overview. In the present work, we only consider the common LMF, i.e. a spin-independent LMF, as this includes spin polarization.[90] Note that we have not included the calibration function[91–93] in eq. 33 for simplicity. Therefore, the exchange part of the XC potential for the Kohn–Sham equations follows as[89]

$$\begin{aligned} V_{\mathrm{X},\mu\nu}^{\mathrm{LHF},\sigma} = &-\frac{1}{2}\int g(\vec{r})D_{\kappa\lambda}^\sigma\left[\chi_\mu\chi_\kappa A_{\nu\lambda}(\vec{r}) + A_{\nu\kappa}(\vec{r})\chi_\mu\chi_\lambda\right] d\vec{r} \\ &+ \int \{1-g(\vec{r})\}\,\hat{d}_{\mu\nu}^\sigma e_{\mathrm{X},\sigma}^\mathrm{sl}\, d\vec{r} \\ &+ \int \hat{d}_{\mu\nu}^\sigma g \times \left[e_{\mathrm{X},\sigma}^\mathrm{HF} - e_{\mathrm{X},\sigma}^\mathrm{sl}\right] d\vec{r} \end{aligned} \tag{34}$$

with the potential operator

$$\hat{d}_{\mu\nu}^\sigma = \sum_{Q\in\mathscr{Q}}\int \frac{\partial Q(\vec{r}')}{\partial P_{\mu\nu}^\sigma}\frac{\partial}{\partial Q(\vec{r}')}\, d\vec{r}' \tag{35}$$

and the matrix A from eq. 21, where the coordinates of the grid points r_g are replaced with the general electronic coordinate r. $\mathscr{Q}$ collects the quantities for the LMF and the DFT energy densities, i.e. $\mathscr{Q} = \{\rho, \vec{\nabla}\rho, \tau, \vec{j}_\mathrm{p}, \dots\}$. The first line is the exact exchange contribution, $K_{\mu\nu}^{\mathrm{LHF},\sigma}$, with the "prefactor" $g(\vec{r})$. Local hybrid functionals are most easily evaluated with a seminumerical ansatz, as all quantities can be evaluated on a grid.[40,94] For the CPKS equations, all non-vanishing terms of the semilocal DFT part only arise through the inclusion of the current density. See also refs. 51,52,54,95 for the CPKS procedure with purely imaginary perturbations. The exact exchange contribution is of a similar form as for global hybrid functionals, however, the prefactor $g(\vec{r})$ needs to be included in the integral, i.e.

$$K_{\mu\nu}^{\mathrm{LHF},\sigma,q} = -\frac{1}{2}\sum_g w_g g(\vec{r}_g)\sum_{\kappa\lambda}\left[X_\mu^g X_\kappa^g A_{\nu\lambda}^g - A_{\nu\kappa}^g X_\mu^g X_\lambda^g\right] P_{\kappa\lambda}^{\sigma,q}. \tag{36}$$

See also ref. 41 for the latest algorithm techniques.

C. Spin-Flip Spin–Orbit Perturbation

The spin-flip contributions for two different spins σ and σ' reads

$$D_{pq}^{\mathrm{SO},\sigma\sigma'} = \frac{1}{S(S-1/2)}\sum_{\mu,\nu} h_{\mu\nu}^{\mathrm{SO},p}\sum_{i,a} c_{\mu i}^{*\sigma} c_{\nu a}^{\sigma'} O_{ai}^{\sigma'\sigma,q}. \tag{37}$$

The spin-flip orbital rotation matrix of the CPKS equations with respect to the spin-orbit perturbation in q direction is given by

$$O_{ai}^{\sigma'\sigma,q} = \frac{F_{ai}^{\sigma'\sigma,q}}{\varepsilon_i^\sigma - \varepsilon_a^{\sigma'}} \tag{38}$$

and is purely imaginary but not purely antisymmetric.[9] The resulting response density matrix for the spin-flip contributions follows as

$$c_{\mu i}^{\sigma,q} = \sum_a c_{\mu a}^{\sigma'} O_{ai}^{\sigma'\sigma,q}, \tag{39}$$

$$P_{\mu\nu}^{\sigma\sigma',q} = \sum_i n_i^{\sigma} c_{\mu i}^{*\sigma} c_{\nu i}^{\sigma,q} + \sum_i n_i^{\sigma'} c_{\mu i}^{*\sigma',q} c_{\nu i}^{\sigma'}. \tag{40}$$

As this response density is purely imaginary but generally non-symmetric, it is convenient to divide it into a symmetric $(+)$ and antisymmetric $(-)$ linear combination for the calculation of the exchange parts. This also means that the CPKS scheme for the calculation of magnetic fields cannot be used as is, but has to be extended for the processing of the symmetric part of the density. Still, the Coulomb part of the CPKS equations vanishes and the same holds for the XC kernel.[9] This is also true for the magnetic XC spin-flip kernel. For the latter, the contributions $-\frac{\vec{j}_{\mathrm{p}}}{4\rho}\frac{\partial f}{\partial \tau}$ and $\frac{|\vec{j}_{\mathrm{p}}|^2}{2\rho^2}$ vanish for any current-free ground state.[53,56]

Within the seminumerical scheme, the exchange part including symmetric and antisymmetric linear combinations follows as

$$K_{\mu\nu}^{\sigma\sigma',\mathrm{sn},+} = \frac{a_{\mathrm{X}}}{2}\sum_g w_g \sum_{\kappa\lambda}\left[X_{\mu}^{g}X_{\kappa}^{g}A_{\nu\lambda}^{g} + A_{\nu\kappa}^{g}X_{\mu}^{g}X_{\lambda}^{g}\right]P_{\kappa\lambda}^{\sigma\sigma',+}, \tag{41}$$

$$K_{\mu\nu}^{\sigma\sigma',\mathrm{sn},-} = \frac{a_{\mathrm{X}}}{2}\sum_g w_g \sum_{\kappa\lambda}\left[X_{\mu}^{g}X_{\kappa}^{g}A_{\nu\lambda}^{g} - A_{\nu\kappa}^{g}X_{\mu}^{g}X_{\lambda}^{g}\right]P_{\kappa\lambda}^{\sigma\sigma',-}. \tag{42}$$

For local hybrids, the exact exchange part with the LMF is again evaluated similarly to global hybrids when only considering spin-independent common LMFs. Only $g(\vec{r})$ needs to be included in the integral and evaluated on a grid, in contrast to the static or constant factor a_{X} for global hybrids. That is, eq. 36 for LHFs is generalized to the spin-flip case just like the static admixture of exact exchange in eq. 26 is generalized to eqs. 41 and 42.

Finally, the total SO contribution to the ZFS tensor reads

$$D_{pq}^{\mathrm{SO}} = D_{pq}^{\mathrm{SO},\alpha} + D_{pq}^{\mathrm{SO},\beta} - D_{pq}^{\mathrm{SO},\alpha\beta} - D_{pq}^{\mathrm{SO},\beta\alpha}. \tag{43}$$

III. IMPLEMENTATION

The approach outlined herein was implemented into the mpshift module[51–53,96–102] of TURBOMOLE.[103–106] The two-electron spin–dipole term was implemented by interfacing the one-electron spin–dipole integrals[107] with the seminumerical routines.[41] Grids for the numerical integration are described in refs. 41 based on the standard DFT grids.[108–110] The non-relativistic framework can make use of the bare one-electron or effective Pauli operators[111,112], the SNSO,[113] and SOMF approach[114,115] for the CPKS SO perturbation. X2C and its local version based on the diagonal local approximation to the unitary decoupling transformation[116,117] support the bare one-electron spin–orbit perturbation matrix as well as the SNSO,[113] mSNSO,[118–120] and SOMF ansätze.[114,115] All integrals for the CPHF/CPKS procedures of the spin–orbit perturbation are taken from previous work[52,115] and one-electron terms can make use of the X2C/DLU-X2C picture-change correction[121] in relativistic calculations, cf. ref. 52 for details. As shown previously, the DLU scheme allows for large-scale calculations while introducing negligible errors for energies,[116,117] gradients,[122] and magnetic properties.[52,98–102,123,124] It was further successfully applied to excitation energies[121,125] and polarizabilities.[121]

Moreover, the CPKS/CPHF approach supports analytical HF or seminumerical HF exchange integrals. The response of the current density and the XC kernel can be included for the same-spin contribution as done previously.[51,52] Density functional approximations are supported up to the class of local hybrid functionals, including the calibration function.[41,49,52,93,126] Further support of density functional expressions is ensured with interfaces to XCFun[127] and Libxc.[128–130] The conductor-like screening model (COSMO) is available to simulate the effect of the environment,[131,132] as it only affects the SCF solution. Just like the Coulomb term, COSMO vanishes for response in the CPKS equations.[97]

Shared-memory parallelization is available throughout with the OpenMP paradigm.[133,134] The implementation was validated by comparison with the numerical example of ref. 9.

IV. COMPUTATIONAL METHODS AND TEST SETS

First, we assess the efficiency and accuracy of the seminumerical integration techniques for the SD term. This is done within the non-relativistic framework with a set of 15 diatomic systems, i.e. O_2, OH^+, S_2, SO, NH, NF, NCl, NBr, PH, PF, SeO, SeS, Se_2, AsH, AsF, and $[Mn(acac)_3]$ with acac = acetylacetonate. Interatomic distances for the diatomic systems are given in the Supporting Information and were taken from the literature.[135] For $[Mn(acac)_3]$, we use the same structure as in ref. 5. Results from ORCA Version 5.0.4[136,137] serve as reference for the SD term, while all other assessments are done with TURBOMOLE. Calculations were performed with the unrestricted Hartree–Fock, BP86,[138,139] and PBE0[140,141] methods. Both programs use the def2-TZVP orbital[142] and auxiliary[143] basis sets for the resolution of the identity approximation (RI-J). In ORCA, we additionally applied the COSX approximation.[36] Default DFT grids are employed with ORCA and medium grids (grid size 3)[108,109] are used with TURBOMOLE. In addition to the direct computation of the SD term, unrestricted natural orbitals[32] are constructed to evaluate the SD term. Coarse (grid size -2) and medium (grid size -1) grids are used for the SD term. See ref. 41 for the grid construction with the seminumerical integration. Additionally, the impact of SNSO and SOMF are studied at the PBE0 level[140,141] for three Ni[144] and V complexes,[145] namely $[Ni(iPrtacn)(NCS)_2]$, $[Ni(iPrtacn)(Cl)_2]$, $[Ni(iPrtacn)(Br)_2]$ with iPrtacn = 1,4,7-triisopropyl-1,4,7-triazacyclononane, and [V(PS3')(1-Me-Im)], [V(PS3')(2,2'-bpy)], $[V(PS3^{H})(1\text{-Me-Im})_3]$ with Me = methyl, PS3' = $P(C_6H_4\text{-5-Me-2-S})_3^{-3}$, $PS3^{H}$ = $P(C_6H_4\text{-2-S})_3^{-3}$, Im = imidazole, bpy = bipyridine. For these complexes, COSMO is used with the default settings, i.e. a permittivity approaching infinity.[131,132] We use the snK approximation for the CPKS equations (grid size -1, medium) and a coarse grid (grid size -2) for the SD term with the UNO approach. Structures are taken from the literature.[144,145]

Wall times are studied for [Mn(acac)$_3$] with various integration grids for the seminumerical scheme at the PBE0/def2-QZVPP[142] level within the SNSO approach. SCF energies are converged up to 10^{-8} E_h and a convergence threshold for the CPKS residuum norm of 10^{-7} is chosen throughout.

Second, meta-GGA and local hybrid functionals are studied for the three Ni[144] and V complexes.[145] Results are compared to "pure" semilocal and (range-separated) hybrid GGA functionals. We consider the BP86,[138,139] PBE0,[140,141] BH&HLYP,[138,146,147] ωB97X-D,[148] B97M,[149] ωB97M,[150] TPSS,[151] TPSSh,[151,152] TPSS0,[151,153] r^{2}SCAN,[60,61] r^{2}SCANh,[60–62] r^{2}SCAN0,[60–62] r^{2}SCAN50,[60–62] M06-L,[57] M06-2X,[58] LH20t,[154] TMHF,[88] and LHJ14[87] functionals with medium grids (grid size 3).[108,109] Inclusion of the paramagnetic current density is indicated by the prefix "c" for the functional, e.g., cTPSS. We use Libxc[128–130] for all functionals except BP86, PBE0, BH&HLYP, TPSS, TPSSh, and LH20t. Other computational settings are the same as for the SNSO study above and the SNSO approach is used. A coarse grid (grid size −2) is employed for the SD term with the UNO approach. For all non-LHFs, we use the snK approximation for the CPKS part (grid size −1, medium). Structures are taken from the literature.[144,145]

Third, we study impact of relativistic effects on 3d, 4d, and 5d complexes, namely the Ni and V complexes as well as [W(CN)$_7$]$^{3-}$, [ReF$_6$]$^{2-}$, [ReCl$_4$(CN)$_2$]$^{2-}$ [ReCl$_4$(ox)]$^{2-}$, [ReBr$_4$(ox)]$^{2-}$, and [MoCl$_2$(DAPBH)] with ox = oxalate, H$_2$DABPBH = 1,1'-(pyridine-2,6-diyl)bis(ethan-1-yl-1-ylidene))dibenzohydrazine. The DLU error for the X2C transformation was previously assessed for various properties and always found to be negligible.[52,98–102,116,117,122–124] Therefore, we only consider X2C in this local approximation. We use the PBE0 functional with medium grids (grid size 3a).[108–110] The non-relativistic and the scalar DLU-X2C Hamiltonian in the finite nucleus model are applied for the SCF procedure. For DLU-X2C, we always use the x2c-TZVPall orbital basis and RI-J auxiliary basis set.[155] For the non-relativistic Hamiltonian, we use the def2-TZVP orbital[142] and auxiliary bases[143] for all elements except W, Re, and Mo. For these elements, the TZVPalls2 basis is employed[98,156] with the x2c-universal auxiliary basis.[155,157] SCF and CPKS equations are converged with thresholds of 10^{-8} E_h and 10^{-7}, respectively. A coarse grid is used for the SD term (grid size −2) in combination with the UNO approach. The SNSO approach is used for the SO term. COSMO is applied with the default parameters.[131,132] Structures are taken from the literature, i.e. we use experimentally determined structures.[158–162] Additionally, the impact of (m)SNSO and SOMF on the DLU-X2C approach are studied for all 12 aforementioned compounds. Furthermore, calculated ZFS parameters for the six 4d/5d compounds are compared to experimental values. For this, we use both experimentally and computationally determined structures. The latter were optimized at the PBE0-D4/def2-TZVP/COSMO level, D4 parameters are taken from ref. 163. For the optimization, an ECP-28 is used for Mo and an ECP-60 is used for Re and W respectively.[164] We apply the BP86,[138,139] PBE0,[140,141] BH&HLYP,[138,146,147] and ωB97X-D[148] functionals and the mSNSO approach for the calculation of the ZFS tensor. Note that the snK approximation is not used for the assessment of relativistic effects, the different SO approaches and for comparison with experiment. The efficiency and accuracy of the snK approach within the X2C framework is assessed for [MoCl$_2$(DAPBH)]. Therefore, the accuracy of the snK approximation in the CPKS equations is explicitly studied in the non-relativistic and the X2C framework.

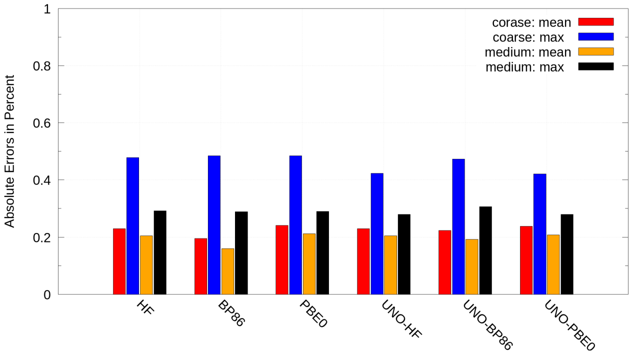

FIG. 1. Mean absolute percent-wise error and maximum percent-wise error with coarse and medium-sized grids for the ZFS D parameter with 15 diatomic systems at different levels of theory. Both the direct approach with the canonical SCF density and the UNO approach are considered. See Supporting Information for the individual data points. The construction of the grids is described in ref. 41.

V. RESULTS AND DISCUSSION

A. Assessment of Efficiency and Accuracy for the Seminumerical Integration and SNSO

First, the accuracy of the seminumerical calculation of the SD term is studied for a set of diatomic compounds and [Mn(acac)$_3$]. The statistical evaluation for the diatomic systems is shown in Fig. 1. Already with the coarse grids described in ref. 41, the error introduced by the seminumerical scheme is clearly negligible, as the mean errors amounts to slightly more than 0.2% and the maximum error is less than 0.5%. The larger medium-sized grid only results in minor improvements for the mean error but maximum errors are almost halved. The findings are virtually the same for the UNO approach and the direct computation of the SD term. The excellent performance of the seminumerical ansatz is confirmed for [Mn(acac)$_3$] in Tab. I. Here, the D and E parameters agree up to 0.002 cm^{-1} and the medium-sized grid alters the results by less than 0.001 cm^{-1}, i.e. the coarse grid already leads to converged results. Therefore, the seminumerical scheme can be safely applied with very small grids.

Second, the SOMF and SNSO ansätze for the CPKS SO part are compared in Tab. II. Both approaches lead to substantially decreased ZFS parameters. Here, the decrease is somewhat larger for SOMF, yet SNSO and SOMF result in very similar D and E values as well as E/D ratios. For instance, the largest absolute change of the D and E parameters upon inclusion of two-electron effects is found for [Ni(iPrtacn)(NCS)$_2$].

TABLE I. SD contributions to the ZFS parameters D and E in cm^{-1} for [Mn(acac)$_3$] with the HF, BP86, and PBE0 method using the def2-TZVP basis set. The SD term is computed with the direct and the UNO approach. The latter is indicated explicitly. Analytical integration is done with ORCA, while the seminumerical (sn) scheme with coarse and medium-sized grids is applied in TURBOMOLE.

Method	SD Integrals	D	E	D (UNO)	E (UNO)
HF	Analytical	−0.529	−0.050	−0.521	−0.045
	Coarse sn	−0.527	−0.051	−0.519	−0.046
	Medium sn	−0.527	−0.051	−0.519	−0.046
BP86	Analytical	−0.355	−0.035	−0.387	−0.036
	Coarse sn	−0.354	−0.035	−0.386	−0.036
	Medium sn	−0.354	−0.035	−0.386	−0.036
PBE0	Analytical	−0.400	−0.038	−0.438	−0.039
	Coarse sn	−0.399	−0.039	−0.437	−0.039
	Medium sn	−0.399	−0.039	−0.437	−0.039

TABLE II. ZFS parameters D and E in cm^{-1} as well as their absolute ratio |E/D| for V and Ni complexes at the PBE0/def2-TZVP/COSMO level. The SD term is computed with the UNO approach. 1e-SO denotes the bare one-electron perturbation.

	[Ni(iPrtacn)(NCS)$_2$]			[V(PS3')(1-Me-Im)]		
SO	D	E	|E/D|	D	E	|E/D|
1e-SO	20.392	6.433	0.315	3.694	0.138	0.037
SNSO	8.340	2.481	0.298	1.610	0.035	0.022
SOMF	6.797	1.977	0.291	1.409	0.025	0.018
	[Ni(iPrtacn)(Cl)$_2$]			[V(PS3')(2,2'-bpy)]		
SO	D	E	|E/D|	D	E	|E/D|
1e-SO	15.510	4.070	0.262	4.480	0.275	0.062
SNSO	6.387	1.574	0.247	1.640	0.076	0.046
SOMF	5.210	1.242	0.239	1.341	0.062	0.047
	[Ni(iPrtacn)(Br)$_2$]			V(PS3H)(1-Me-Im)$_3$]		
SO	D	E	|E/D|	D	E	|E/D|
1e-SO	15.525	3.441	0.222	2.092	0.366	0.175
SNSO	6.681	1.296	0.194	0.884	0.169	0.191
SOMF	5.438	1.032	0.190	0.757	0.150	0.198

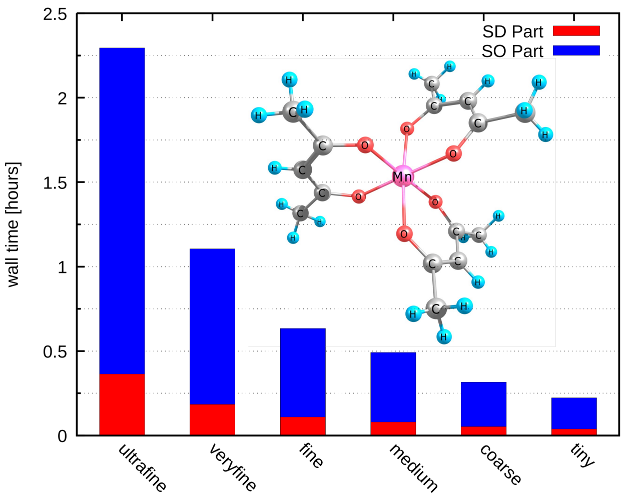

FIG. 2. Wall times for the SD and SO contributions of [Mn(acac)$_3$] at the PBE0/def2-QZVPP level in hours. We use the UNO ansatz for the SD term and SNSO approach for the SO term. Note that the analytical integrals for HF exchange of the SO term lead to a SO computation time of 7.3 hours. Calculations were carried out with a CPU of type AMD EPYC 7453 utilizing a total of 8 OpenMP threads. The code was compiled with the ifx (IFORT) compiler, version 2022.1.0. See Supporting Information for details and the ZFS parameters.

Here, the D value changes from 20.392 (1e-SO) to 8.340 (SNSO) and 6.797 cm^{-1} (SOMF). This is a change of around 12.1 and 13.6 cm^{-1} respectively. For the E value, SNSO and SOMF lead to a decrease of about 4.0 and 4.5 cm^{-1} respectively. Thus, SNSO accurately models the two-electron contribution of the spin–orbit interaction.

Third, the efficiency of the seminumerical ansatz for the SD and SO contribution are assessed for [Mn(acac)$_3$] at the PBE0/def2-QZVPP level. Here, the complete ZFS calculation with SOMF (analytical integrals for all CPKS steps) and the UNO approach for the SD term (coarse grid) takes about 13.7 hours with a central processing unit (CPU) of type AMD EPYC 7453 utilizing a total of 8 OpenMP threads, while the corresponding SNSO ansatz only requires 7.3 hours. The SCF procedure takes 2.5 hours for 44 iterations without COSMO and 2.3 hours for 41 iterations with COSMO (initial guess from superposition of atomic densities with Hückel orbitals and occupations[165]). Results for the ZFS parameters are −2.6965 for D and −0.2656 cm^{-1} for E with SOMF compared to −3.1766 and −0.3165 cm^{-1} with SNSO. Thus, SNSO again yields similar results as SOMF at notably reduced costs. Further speedups are possible with the snK approximation for the SO term. Timings for the SD and SO terms with all grids are shown in Fig. 2. Even with the largest grid, ultrafine, the computation of the SD requires only around 22 minutes and is consequently cheap compared to the total ZFS calculation. The computation time becomes completely negligible with the tiny grid, i.e. it amounts to just 2 minutes. Application of the snK approximation for the CPKS equations of the SO contribution leads to drastic speedups of the computation time. Already the ultrafine grid results in a speedup for the SO contribution by more than a factor of 3, i.e. the computation time is reduced from around 7.3 to around 2.0 hours. Up to the medium-sized grid the errors for D and E amount to only 0.0001 and 0.0010 cm^{-1} respectively, but an acceleration with a factor of more than 17 is observed for the SO part. The total wall time is reduced from 7.3 to less than 0.5 hours while introducing clearly negligible errors. This way, the SCF calculation is the time-determining step. As a final note, the impact of the def2-QZVPP basis on the results in comparison with the def2-TZVP basis is negligible as shown in the Supporting Information. Therefore, it is sufficient here to use bases in TZVP quality. Nevertheless, the results for the seminumerical networks are valid in terms of efficiency and accuracy also for smaller basis sets. However, the gain in computation time decreases compared to the analytical evaluation for smaller basis sets.[40]

TABLE III. ZFS parameters D and E in cm^{-1} as well as their absolute ratio $|E/D|$ for three Ni complexes. The SNSO spin-orbit perturbation operator is applied and the SD term is computed with the UNO approach. Experimental references (Expt.) based on frequency-domain magnetic resonance spectroscopy are taken from ref. 144.

	[Ni(iPrtacn)(NCS)$_2$]			[Ni(iPrtacn)(Cl)$_2$]			[Ni(iPrtacn)(Br)$_2$]		
	D	E	$\|E/D\|$	D	E	$\|E/D\|$	D	E	$\|E/D\|$
Expt.	15.9	4.9	0.31	15.9	3.2	0.20	13.8	3.3	0.24
BP86	3.702	0.735	0.199	3.066	0.534	0.174	3.732	0.506	0.136
PBE0	8.340	2.481	0.298	6.387	1.574	0.247	6.681	1.296	0.194
BH&HLYP	14.885	4.834	0.325	11.404	2.969	0.260	10.338	2.511	0.243
ωB97X-D	9.873	3.145	0.319	7.745	2.141	0.277	8.065	1.756	0.218
B97M	0.845	0.067	0.079	0.551	0.022	0.040	0.754	0.102	0.136
cB97M	8.086	1.749	0.216	6.418	1.005	0.157	6.353	1.080	0.170
ωB97M	4.624	1.094	0.237	3.437	0.719	0.209	3.928	0.697	0.177
cωB97M	10.204	2.902	0.284	7.827	1.860	0.238	7.972	1.627	0.204
TPSS	2.167	0.347	0.160	1.633	0.210	0.129	2.104	0.240	0.114
cTPSS	3.964	0.851	0.215	3.172	0.552	0.174	3.642	0.473	0.130
TPSSh	2.914	0.596	0.205	2.136	0.356	0.166	2.636	0.297	0.113
cTPSSh	5.162	1.271	0.246	4.009	0.794	0.198	4.415	0.659	0.149
TPSS0	4.506	1.120	0.249	3.256	0.661	0.203	3.478	0.595	0.171
cTPSS0	7.501	2.069	0.276	5.678	1.249	0.220	5.634	1.089	0.193
r^{2}SCAN	1.182	0.131	0.111	0.782	0.024	0.031	1.080	0.160	0.148
cr^{2}SCAN	6.378	1.496	0.235	4.888	0.778	0.159	5.145	0.818	0.159
r^{2}SCANh	1.512	0.204	0.135	1.009	0.060	0.059	1.302	0.122	0.094
cr^{2}SCANh	7.343	1.810	0.247	5.551	0.941	0.169	5.602	0.965	0.172
r^{2}SCAN0	2.307	0.409	0.177	1.569	0.172	0.110	1.739	0.236	0.136
cr^{2}SCAN0	9.144	2.396	0.262	6.820	1.254	0.184	6.457	1.246	0.193
r^{2}SCAN50	5.430	1.342	0.247	3.863	0.690	0.179	3.566	0.711	0.199
cr^{2}SCAN50	13.892	4.073	0.293	10.420	2.199	0.211	9.149	2.030	0.222
M06-L	1.512	0.206	0.136	0.989	0.059	0.060	1.635	0.231	0.141
cM06-L	6.903	1.689	0.245	5.169	0.702	0.136	5.886	1.164	0.198
M06-2X	1550.294	211.068	0.136	−2410.015	−626.640	0.260	−2571.018	−268.028	0.104
cM06-2X	−25.448	−5.703	0.224	−21.295	−5.832	0.274	7.137	0.959	0.134
LH20t	−12.305	−4.100	0.333	10.217	2.907	0.285	9.848	2.050	0.208
cLH20t	11.045	3.608	0.327	9.139	2.548	0.279	8.860	1.808	0.204
TMHF	7.483	2.031	0.271	6.016	1.351	0.225	6.575	1.152	0.175
cTMHF	5.540	1.342	0.242	4.364	0.867	0.199	4.936	0.781	0.158
LHJ14	6.765	1.747	0.258	5.770	1.313	0.228	6.672	0.953	0.143
cLHJ14	3.247	0.541	0.167	2.579	0.405	0.157	3.370	0.297	0.088

In conclusion, the seminumerical integration techniques introduce negligible errors already with coarse grids and lead to substantial speedups of the computation time. This confirms our previous studies with the snK approximation for various magnetic properties and basis sets,[49,52,102,124] and shows again that small grids are generally sufficient for response properties. SNSO and SOMF lead to similar results but the computational demands differ significantly. The latter dominates the computation time compared to the seminumerical schemes for the other integrals, and therefore, the SNSO approach is computationally advantageous.

B. Importance of the Current Density for Meta-GGAs and Local Hybrids

Results for three nickel and vanadium complexes are shown in Tab. III and IV, respectively. Here, the common hybrid GGA functionals PBE0 and ωB97X-D perform reasonable well for the D and E parameters. These hybrid functionals are a notable improvement upon the semilocal GGA BP86. A large amount of exchange with BH&HLYP (50%) yields excellent results for the three Ni complexes and also performs well for the V complexes.

For the nickel complexes, most functionals underestimate the ZFS parameters, i.e. only the results with BH&HLYP, r^{2}SCAN50, ωB97M, and LH20t substantially cross the $10\,\mathrm{cm}^{-1}$ mark. For [Ni(iPrtacn)(NCS)$_2$], very good agreement is found with BH&HLYP. Here, the D and E values are very close to the experimental results. For [Ni(iPrtacn)(Cl)$_2$] and [Ni(iPrtacn)(Br)$_2$], somewhat larger deviations of around 1 to $4.5\,\mathrm{cm}^{-1}$ for D are observed, however, the results for E are again close to experimental results. Note that BH&HLYP already performed excellent for magnetizabilities.[166,167] Thus, the good performance is not completely unexpected.

For the meta-GGAs, TPSS leads to similar results as the GGA BP86 and the admixture of exact exchange leads to an increase of D and E. However, the amount of exact exchange

TABLE IV. ZFS parameters D and E in cm^{-1} as well as their absolute ratio $|E/D|$ for three V complexes. The SNSO spin-orbit perturbation operator is applied and the SD term is computed with the UNO approach. Experimental references (Expt.) taken from ref. 145.

	[V(PS3')(1-Me-Im)]			[V(PS3')(2,2'-bpy)]			[V(PS3H)(1-Me-Im)$_3$]		
	D	E	|E/D|	D	E	|E/D|	D	E	|E/D|
Expt.	1.80	0.047	0.03	1.70	0.075	0.04	0.96	0.19	0.20
BP86	1.327	0.011	0.008	1.143	0.023	0.020	0.945	0.111	0.117
PBE0	1.610	0.035	0.022	1.640	0.076	0.046	0.884	0.169	0.191
BH&HLYP	1.963	0.064	0.033	1.902	0.068	0.036	0.815	0.220	0.270
ωB97X-D	1.779	0.038	0.022	1.720	0.068	0.040	0.934	0.175	0.188
B97M	1.164	0.006	0.005	0.828	0.041	0.050	0.567	0.097	0.171
cB97M	1.147	0.059	0.052	1.466	0.126	0.086	0.787	0.242	0.308
ωB97M	1.731	0.036	0.021	1.633	0.074	0.045	0.857	0.173	0.202
cωB97M	1.918	0.056	0.029	2.022	0.084	0.041	0.876	0.230	0.262
TPSS	1.160	0.008	0.007	0.939	0.021	0.022	0.758	0.091	0.120
cTPSS	1.100	0.017	0.016	1.004	0.034	0.034	0.777	0.120	0.155
TPSSh	1.247	0.012	0.010	1.036	0.037	0.036	0.744	0.105	0.141
cTPSSh	1.227	0.024	0.020	1.173	0.044	0.037	0.762	0.138	0.181
TPSS0	1.353	0.022	0.017	1.170	0.047	0.040	0.714	0.128	0.180
cTPSS0	1.398	0.038	0.027	1.400	0.054	0.039	0.735	0.166	0.226
r^{2}SCAN	1.173	0.006	0.005	0.922	0.031	0.034	0.693	0.102	0.147
cr^{2}SCAN	1.099	0.040	0.037	1.298	0.098	0.076	0.799	0.217	0.271
r^{2}SCANh	1.245	0.010	0.008	0.997	0.043	0.043	0.697	0.114	0.163
cr^{2}SCANh	1.292	0.050	0.039	1.537	0.096	0.063	0.805	0.234	0.291
r^{2}SCAN0	1.343	0.018	0.014	1.113	0.051	0.046	0.694	0.134	0.193
cr^{2}SCAN0	1.559	0.067	0.043	1.832	0.096	0.052	0.816	0.257	0.316
r^{2}SCAN50	1.592	0.045	0.028	1.473	0.050	0.034	0.702	0.184	0.263
cr^{2}SCAN50	1.959	0.097	0.050	2.239	0.100	0.045	−0.875	−0.285	0.326
M06-L	1.528	0.013	0.008	1.355	0.055	0.041	0.963	0.138	0.143
cM06-L	1.691	0.065	0.038	2.163	0.156	0.072	1.235	0.319	0.258
M06-2X	4.812	0.435	0.090	18.665	4.691	0.251	−3.273	−0.947	0.290
cM06-2X	2.246	0.019	0.008	1.935	0.316	0.163	1.215	0.130	0.107
LH20t	1.828	0.044	0.024	1.886	0.094	0.050	0.966	0.185	0.192
cLH20t	1.809	0.035	0.019	1.740	0.084	0.048	0.967	0.164	0.170
TMHF	1.901	0.036	0.019	1.891	0.095	0.050	1.096	0.177	0.162
cTMHF	1.890	0.022	0.011	1.667	0.083	0.050	1.100	0.137	0.125
LHJ14	1.746	0.024	0.014	1.637	0.068	0.041	1.084	0.148	0.137
cLHJ14	1.818	0.007	0.004	1.428	0.062	0.043	1.102	0.098	0.089

in TPSSh (10%) is too small for a substantial improvement, e.g., the D values for [Ni(iPrtacn)(NCS)$_2$] changes from 3.964 to 5.162 cm^{-1}, while ωB97X-D yields D = 9.873 cm^{-1}. Increasing the amount of exact exchange to 25% with TPSS0 further improves the results to 7.501 cm^{-1}. To compare, the experimental finding is 15.9 cm^{-1}. A similar trend is observed for the other complexes.

The current density notably affects the ZFS parameters as shown by B97M, ωB97M, M06-L, and the r^{2}SCAN functionals. Here, the values for D increase by about 4 to 8 cm^{-1}. A dramatic case is M06-2X. Without the current density, the results are completely unreasonable and off by orders of magnitude, i.e. the absolute values of the D and E parameters are larger than 1500 and 200 cm^{-1}. This is entirely caused by the SO contribution, as the result for the SD term is in the usual range. Accounting for the current density leads to drastic changes in the correct direction, but still the results obtained with this functional are worse than most of the results of the other functionals. We note that grid sensitivities and numerical instabilities may also be detrimental for some functionals.[168] Thus, we re-calculated the ZFS parameters for [Ni(iPrtacn)(Cl)$_2$] and M06-2X with the reference grid settings[165] and analytical HF exchange. The respective D and E parameters are 2023.298 and 626.611 cm^{-1}. $|E/D|$ is close to one third and the sign determination is consequently unreliable, as small changes in the actual tensor components can lead to a sign flip. Thus, this functional is also very sensitive towards the grid. Overall, the inclusion of the current density for τ is clearly mandatory for almost all functional families and the current density improves the results for all meta-GGAs.

Local hybrid functionals such as LH20t, TMHF, and LHJ14 lead to increased computational costs[49] and do not show major improvements over conventional global hybrid or range-separated functionals for the ZFS. Here, the current density leads to a decrease of the D and E parameters and consequently worsens the results. Without the current density, TMHF performs similar to PBE0, while LH20t is clearly off for one of the three complexes. This can again be rationalized by the E/D ratio being close to one third. When the current density is included, LH20t yields good results for all three complexes. Note that LH20t is constructed with a so-called t-LMF relying on the iso-orbital indicator. Only with the proper generalization of τ, the von-Weizäcker inequality and the iso-orbital constraint are restored. Therefore, the inclusion of the current density is formally required for LH20t and related functionals such as, e.g., LH12ct-SsirPW92.[90]

For the vanadium complexes, the ZFS parameters are much smaller and ωB97X-D results in an excellent agreement with the experiment. Again, TPSS underestimates the D and E values and TPSSh leads to a minor increase in line with the small amount of exact exchange added. The impact of the current density is less pronounced for M06-L and r^{2}SCAN, however, it is still of major importance for M06-2X. The wrong sign of the D parameter of [V(PS3H)(1-Me-Im)$_3$] with r^{2}SCAN50 is again due to the E/D ratio being close to one third. The local hybrids LH20t or TMHF are in good agreement with the experimental results for D, considerably improving upon their mediocre performance observed for the Ni complexes. However, the predicted E/D ratios are altogether worse than the values obtained from the global hybrid PBE0 or the range-separated hybrid ωB97X-D.

In conclusion, the results show that DFT can yield very good results for the ZFS of 3d complexes when used with the formalism of the van Wüllen group from ref. 9. The bad or unfavorable performance of DFT discussed in refs. 145,169,170 may be at least partly attributed to the CP-SOC formalism. BH&HLYP performs best for the studied complexes and leads to excellent results compared to the experiment. ωB97X-D and r^{2}SCAN50 rank second, as they too give reasonable results for all the considered compounds. This confirms the robust performance of ωB97X-D found for EPR parameters in previous studies.[52,100,101] Further, the current density generally needs to be included for meta-GGAs, especially for the Minnesota functionals and r^{2}SCAN. Semilocal meta-GGAs offer some improvements over BP86, however, hybrid functionals are usually a better option. Here, the increased flexibility of local hybrids shows some potential but does not yet lead to an overall better performance. The DFT framework could formally be improved for the two-electron SD term, which is currently evaluated as done for Hartree–Fock theory.[9]

C. Application to Heavy Elements with X2C

First, the impact of X2C is assessed with results shown in Tab. V for 4d and 5d complexes. See Supporting Information for results with the 3d complexes. As expected, DLU-X2C and the non-relativistic framework lead to very similar results for the 3d complexes. The deviations amount to less than 0.1 cm^{-1} for the D parameters of both the Ni complexes and V complexes. In contrast, somewhat larger changes are observed for the heavier elements. Here, the non-relativistic ansatz is clearly insufficient for [W(CN)$_7$]$^{3-}$. The small impact of X2C for some complexes can be rationalized by the two contributions to the ZFS, i.e. scalar effects on the SCF density and the picture-change correction of the SO perturbation. These effects can cancel each other to some extent. To illustrate this, we consider the D parameter of [ReF$_6$]$^{2-}$. Here, the non-relativistic framework leads to −15.524 cm^{-1}, while DLU-X2C with and without the SO picture-change correction gives 14.307 cm^{-1} and 15.930 cm^{-1}, respectively. In fact, the NR approach benefits from error cancellation for all Re complexes. Note that this finding is not restricted to the ZFS but was already observed for NMR shifts.[171,172] Overall, the inclusion of scalar relativistic effects for the SCF density and the relativistic picture-change correction for the SO perturbation are desirable for 5d complexes.

Second, results for the comparison of the SO approaches

TABLE V. ZFS parameters D and E in cm^{-1} as well as their absolute ratio $|E/D|$ for Mo, W, and Re complexes at the PBE0/COSMO level using the non-relativistic Hamiltonian (NR) or the scalar DLU-X2C Hamiltonian for the SCF procedure. DLU-X2C utilizes the x2c-TZVPall bases, while the NR results are obtained with the TZVPalls2 (W, Re, Mo) and the def2-TZVP (other elements) basis sets. The SD term is computed with the UNO approach and the SNSO approximation is applied. Inclusion of the relativistic picture-change correction (pcc) is explicitly denoted. We do not use the snK approximation for this study. See Supporting Information for the Ni and V complexes.

	[W(CN)$_7$]$^{3-}$		
Hamiltonian	D	E	$\lvert E/D\rvert$
NR	253.290	0.047	0.000
DLU-X2C (no pcc)	237.319	0.052	0.000
DLU-X2C (pcc)	219.012	0.054	0.000

	[ReF$_6$]$^{2-}$		
Hamiltonian	D	E	$\lvert E/D\rvert$
NR	−15.524	−4.999	0.322
DLU-X2C (no pcc)	−15.930	−5.156	0.324
DLU-X2C (pcc)	−14.307	−4.623	0.323

	[ReCl$_4$(CN)$_2$]$^{2-}$		
Hamiltonian	D	E	$\lvert E/D\rvert$
NR	−36.839	−0.905	0.025
DLU-X2C (no pcc)	−37.474	−0.960	0.026
DLU-X2C (pcc)	−34.177	−0.853	0.025

	[ReCl$_4$(ox)]$^{2-}$		
Hamiltonian	D	E	$\lvert E/D\rvert$
NR	−55.982	−17.062	0.305
DLU-X2C (no pcc)	−56.474	−17.703	0.314
DLU-X2C (pcc)	−51.058	−15.850	0.310

	[ReBr$_4$(ox)]$^{2-}$		
Hamiltonian	D	E	$\lvert E/D\rvert$
NR	−62.577	−16.438	0.263
DLU-X2C (no pcc)	−68.601	−20.013	0.292
DLU-X2C (pcc)	−62.259	−18.127	0.291

	[MoCl$_2$(DAPBH)]		
Hamiltonian	D	E	$\lvert E/D\rvert$
NR	42.596	0.489	0.012
DLU-X2C (no pcc)	40.266	0.434	0.011
DLU-X2C (pcc)	39.362	0.424	0.011

TABLE VI. ZFS parameters D and E in cm^{-1} as well as their absolute ratio |E/D| for six V, Ni, W, Re, and Mo complexes (PBE0/x2c-TZVPall/DLU-X2C level). The SD term is computed with the UNO approach. 1e-SO denotes the bare one-electron perturbation. We include the relativistic picture-change correction (DLU-X2C) for all one-electron terms and the SNSO and mSNSO approximation are applied.

	$[\mathrm{Ni(iPrtacn)(NCS)}_2]$			$[\mathrm{Ni(iPrtacn)(Cl)}_2]$			$[\mathrm{Ni(iPrtacn)(Br)}_2]$		
	D	E	|E/D|	D	E	|E/D|	D	E	|E/D|
1e-SO	20.472	6.419	0.314	15.379	3.947	0.257	15.371	3.365	0.219
SNSO	8.361	2.471	0.296	6.331	1.523	0.241	6.624	1.265	0.191
mSNSO	7.450	2.178	0.292	5.647	1.342	0.238	5.946	1.110	0.187
SOMF	6.742	1.949	0.289	5.109	1.187	0.232	5.337	0.997	0.187

	[V(PS3’)(1-Me-Im)]			[V(PS3’)(2,2’-bpy)]			$[\mathrm{V(PS3H)(1\text{-}Me\text{-}Im)}_3]$		
	D	E	|E/D|	D	E	|E/D|	D	E	|E/D|
1e-SO	3.649	0.134	0.037	4.391	0.265	0.060	2.105	0.355	0.169
SNSO	1.586	0.034	0.021	1.609	0.069	0.043	0.885	0.164	0.186
mSNSO	1.449	0.027	0.019	1.419	0.060	0.042	0.798	0.151	0.189
SOMF	1.382	0.024	0.017	1.309	0.056	0.042	0.751	0.145	0.193

	$[\mathrm{W(CN)}_7]^{3-}$			$[\mathrm{ReF}_6]^{2-}$			$[\mathrm{ReCl}_4\mathrm{(CN)}_2]^{2-}$		
	D	E	|E/D|	D	E	|E/D|	D	E	|E/D|
1e-SO	296.331	0.074	0.000	−19.135	−6.169	0.322	−45.205	−1.145	0.025
SNSO	219.012	0.054	0.000	−14.307	−4.623	0.323	−34.177	−0.853	0.025
mSNSO	211.940	0.052	0.000	−13.858	−4.481	0.323	−33.045	−0.827	0.025
SOMF	188.585	0.047	0.000	−12.468	−4.035	0.324	−29.730	−0.744	0.025

	$[\mathrm{ReCl}_4\mathrm{(ox)}]^{2-}$			$[\mathrm{ReBr}_4\mathrm{(ox)}]^{2-}$			$[\mathrm{MoCl}_2\mathrm{(DAPBH)}]$		
	D	E	|E/D|	D	E	|E/D|	D	E	|E/D|
1e-SO	−68.523	−21.327	0.311	−84.032	−25.297	0.301	66.449	0.752	0.011
SNSO	−51.058	−15.850	0.310	−62.259	−18.127	0.291	39.362	0.424	0.011
mSNSO	−49.439	−15.359	0.311	−60.259	−17.501	0.290	36.999	0.398	0.011
SOMF	−44.423	−13.801	0.311	−54.047	−15.650	0.290	33.177	0.360	0.011

TABLE VII. ZFS parameters D and E in cm^{-1} as well as their absolute ratio |E/D| for W, Re, and Mo complexes (x2c-TZVPall/DLU-X2C/COSMO level). The mSNSO spin-orbit perturbation ansatz is applied, including the picture-change correction, and the SD term is computed with the UNO approach. Experimental findings (Expt.) are taken from refs. 158–162. There are two experimental results for $[\mathrm{W(CN)}_7]^{3-}$.[159] Further results with the computationally optimized structures are given in the Supporting Information. These results are qualitatively similar for all compounds except $[\mathrm{ReF}_6]^{2-}$, where the computationally optimized structure is O_h symmetric and the ZFS parameters are close to zero.

	$[\mathrm{W(CN)}_7]^{3-}$			$[\mathrm{ReF}_6]^{2-}$			$[\mathrm{ReCl}_4\mathrm{(CN)}_2]^{2-}$		
	D	E	|E/D|	D	E	|E/D|	D	E	|E/D|
Expt.	330, 430	110, 41	0.33, 0.10	23.6	2.6	0.11	−14.4	–	–
BP86	218.663	0.031	0.000	−14.034	−4.493	0.320	−42.111	−0.840	0.020
PBE0	211.940	0.052	0.000	−13.858	−4.481	0.323	−33.045	−0.827	0.025
BH&HLYP	249.853	0.080	0.000	−15.647	−5.065	0.324	−30.624	−1.101	0.036
ωB97X-D	274.546	0.058	0.000	−15.792	−5.141	0.326	−36.155	−1.118	0.031

	$[\mathrm{ReCl}_4\mathrm{(ox)}]^{2-}$			$[\mathrm{ReBr}_4\mathrm{(ox)}]^{2-}$			$[\mathrm{MoCl}_2\mathrm{(DAPBH)}]$		
	D	E	|E/D|	D	E	|E/D|	D	E	|E/D|
Expt.	−53	−14	0.26	−73	−15	0.205	50	0.025	0.00
BP86	−52.092	−15.265	0.293	−61.954	−13.010	0.210	35.759	0.280	0.008
PBE0	−49.439	−15.359	0.311	−60.259	−17.501	0.290	36.999	0.398	0.011
BH&HLYP	−52.057	−17.251	0.331	66.834	21.296	0.319	40.976	0.495	0.012
ωB97X-D	−54.461	−17.243	0.317	−67.443	−20.329	0.301	45.053	0.450	0.010

are listed in Tab. VI. A consideration of the two-electron terms either effectively with SNSO/mSNSO or explicitly with SOMF leads to a notable decrease of the ZFS parameters for all complexes (in absolute numbers). For instance, the

D parameter of $[W(CN)_7]^{3-}$ decreases from 296 with the bare one-electron SO approach (1e-SO) to 188 cm^{-1} with SOMF. SNSO and mSNSO are intermediate cases with 219 and 212 cm^{-1}. Generally, mSNSO leads to a better agreement with SOMF than the original SNSO ansatz. However, the deviation between SNSO and mSNSO is relatively small. These findings are in qualitative agreement with similar studies for the EPR hyperfine coupling constants and g-tensors, where the mSNSO/SNSO approaches also agreed well with two-electron spin–orbit mean field ansätze[173] and four-component approaches.[100,101] Compared to the impact of all other computational parameters studied in the previous sections, the mSNSO approximation is well balanced in terms of accuracy and efficiency, as it does not increase the computational costs compared to the 1e-SO formulation at all. Thus, we recommend this approach for large-scale X2C calculations with density functional methods, while SOMF may be beneficial for correlated wavefunction-based approaches.

Third, the mSNSO-DLU-X2C approach is assessed in comparison with the experimental findings in Tab. VII. As X2C did not notably affect the results for the Ni and V complexes, we only show results for the 4d and 5d complexes in the main text. For $[ReCl_4(ox)]^{2-}$, $[ReBr_4(ox)]^{2-}$, and $[MoCl_2(DAPBH)]$, we obtain good results with the considered density functionals. This holds for the D and E parameters as well as their ratio with the exception of the BH&HLYP results for $[ReBr_4(ox)]^{2-}$. Here, the E/D ratio is close to one third and the sign of D and E is not correctly reproduced, similar to previous observations in Sec. V B. In contrast to the good performance for these three compounds, the results for $[W(CN)_7]^{3-}$, $[ReF_6]^{2-}$, or $[ReCl_4(CN)_2]^{2-}$ show a notable deviation towards the experiment. This is especially true for $[W(CN)_7]^{3-}$, where none of the functionals yields a E parameter larger than 1 cm^{-1} and the ratio of D and E is essentially zero. The two experimental approaches for this complex lead to very different results, however, the E parameters are 110 and 38 cm^{-1} and consequently not zero. For $[ReF_6]^{2-}$, the ratio $|E/D|$ is again the main reason for the wrong signs of the D and E parameters.

Fourth, we apply the snK approximation and study the grid dependence for $[MoCl_2(DAPBH)]$. Timings with different grids for the seminumerical schemes of the SD and SO contributions are shown in Fig. 3. Already the largest grid results in a slight speedup compared to the analytical integration for the SO part, which dominates the computation time. In detail, the analytical exchange integrals result in a computation time for the SO contribution of 59.7 minutes and this time is reduced to 41.7 minutes with the ultrafine grid. The next grid (veryfine) already halves the computation time. Note that the error amounts to less than 0.01 cm^{-1} for the SD term and less than 0.1 cm^{-1} for the SO contribution (D parameter) up to the coarse grid. The tiny grid leads to errors of 0.03 and 0.4 cm^{-1}, respectively. Therefore, the coarse grid can be safely used with substantial speedups, i.e. wall times are reduced by a factor of 7 compared to the ultrafine grid. Especially the time needed to compute the SO contribution can be significantly reduced by the seminumerical integration. This shows that the seminumerical scheme performs excellently within a non-relativistic and a relativistic framework.

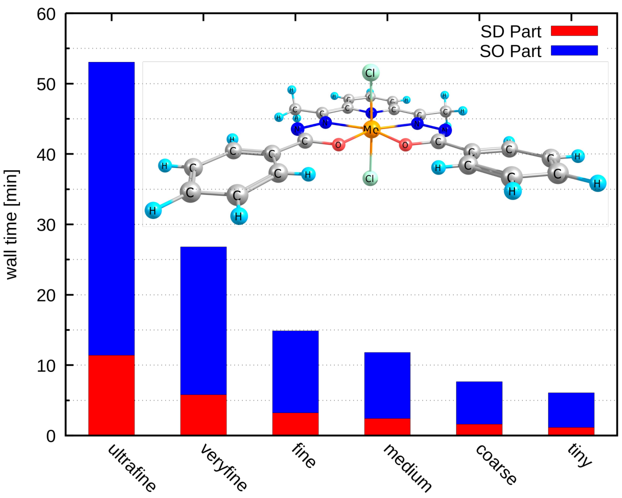

FIG. 3. Wall times for the SD and SO contributions of $[MoCl_2(DAPBH)]$ at the PBE0/x2c-TZVPall/DLU-X2C/COSMO level of theory in minutes. To compare, the analytical integrals for the SO contributions result in a wall time of 59.7 minutes. Calculations were carried out with a CPU of type AMD EPYC 7453 utilizing a total of 8 OpenMP threads. The code was compiled with the ifx (IFORT) compiler, version 2022.1.0. See Supporting Information for details and the ZFS parameters.

In conclusion, relativistic effects can be included with minimal computational costs at the DLU-X2C level. The seminumerical approaches require no special grids and coarse grids are still sufficient for accurate results.

VI. SUMMARY AND CONCLUSIONS

We presented an efficient implementation of the zero-field splitting (ZFS) tensor up to the class of meta-generalized gradient approximations (meta-GGAs) and local hybrid functionals including the paramagnetic current density for the kinetic-energy density. Our work consequently generalizes the formalism discussed in ref. 9. The key ingredient for efficiency is a seminumerical scheme for the two-electron integrals, which leads to drastic speedups without introducing any notable errors, even with very small integration grids. It is found that the current density is of great importance for the ZFS parameters with almost all meta-GGAs considered herein, namely the B97M, SCAN, Minnesota, and TPSS functional families. Together with previous studies for magnetic properties,[49–54] this shows that the inclusion of the current density becomes more and more important with the number of unpaired electrons.

Furthermore, the spin–orbit perturbation is formulated with an exact two-component (X2C) approach making use of the screened nuclear spin–orbit (SNSO) correction. This leads to similar results as the spin–orbit mean field (SOMF) ansatz, while substantially reducing the computational costs. Therefore, our work enables relativistic large-scale calculations with low computational demands.

Moreover, we have shown that common density functional approximations can lead to a reasonable agreement with the experiment for the ZFS parameters, in contrast to the studies of refs. 145,169,170. However, larger deviations form experiment were observed for some 5d compounds. Additionally, it should be stressed that the calculated sign of the D parameter becomes unreliable, if the |E/D| ratio is close to one third.

As an outlook, the ZFS developments herein can be combined with our previous work on EPR hyperfine coupling constants[99,100] and g-tensors[52,101] to compute the paramagnetic NMR shielding tensor of systems with more than one unpaired electron[25–28] based on X2C and current-dependent density functional approximations.

SUPPLEMENTARY MATERIAL

Supporting Information is available with the structures optimized in this work (txt file) and complete data (xlsx file).

ACKNOWLEDGMENTS

The authors thank Christoph van Wüllen for providing ZFS results of Se_2 for comparison and validation. We gratefully acknowledge support from the Deutsche Forschungsgemeinschaft (DFG, German Research Foundation) through the Collaborative Research Centre “4f for Future” (CRC 1573 project no. 471424360, project Q) Y.J.F. acknowledges financial support by Turbomole GmbH. C.H. gratefully acknowledges funding by the Volkswagen Foundation.

DATA AVAILABILITY STATEMENT

The data that support the findings of this study are available within the article and its supplementary material.

Conflict of Interest

The authors have no conflicts to disclose.

Appendix A: Spin–Orbit Perturbation Approaches

For light elements, the bare one-electron Pauli spin–orbit operator on top of a non-relativistic SCF procedure reads

$$\begin{aligned}\hat{H}^{\mathrm{SO}} &= \sum_i \hat{h}^{\mathrm{SO}}(i) = \sum_i \hat{\vec{h}}^{\mathrm{SO}}(i)\cdot\hat{\vec{s}}(i)\\ &= \frac{\mathrm{i}}{2c^2}\sum_i\left[\hat{\vec{p}}(i)\,\hat{V}(i)\times\hat{\vec{p}}(i)\right]\cdot\hat{\vec{s}}(i)\end{aligned}\tag{A1}$$

with i denoting the electrons, i the imaginary unit number, $\hat{V}$ the electron-nucleus potential, and $\hat{\vec{s}}$ the spin operator. In the point-charge model, we may further simplify $\hat{\vec{h}}^{\mathrm{SO}}$ to

$$\hat{\vec{h}}^{\mathrm{SO}}(i) = \frac{1}{2c^2}\sum_N Z_N r_{iN}^{-3}\left[\vec{r}_{iN}\times\hat{\vec{p}}(i)\right]\tag{A2}$$

with the charge Z_N of a nucleus N. The spin-dependent operator $\hat{h}^{\mathrm{SO}}(i)$ leads to the matrix elements

$$h^{\mathrm{SO}}_{\mu\nu} = \frac{\mathrm{i}}{4c^2}\langle\mu|\vec{\sigma}\cdot\left(\hat{\vec{p}}\,\hat{V}\times\hat{\vec{p}}\right)|\nu\rangle\,,\tag{A3}$$

making use of the relation $\hat{\vec{s}} = 1/2\vec{\sigma}$ with the vector $\vec{\sigma}$ collecting the three Pauli spin matrices. The qth component of this Hamiltonian is then given by

$$h^{\mathrm{SO},q}_{\mu\nu} = \frac{\mathrm{i}}{4c^2}\langle\mu|\left(\hat{\vec{p}}\,\hat{V}\times\hat{\vec{p}}\right)_q|\nu\rangle\,,\tag{A4}$$

To account for the effect of spin–orbit coupling on the two-electron interaction, the nuclear charge Z for the potential $\hat{V}$ may be replaced with an effective charge.[111,112] Alternatively, we may apply the screened-nuclear spin–orbit (SNSO) approach.[113] This was initially proposed for low-order Douglas–Kroll–Hess theory[174–176] but can also be applied within a non-relativistic framework. Then, the spin–orbit perturbation matrix reads

$$\begin{aligned}h^{\mathrm{SNSO}}_{\mu\nu} = &\ \frac{\mathrm{i}}{4c^2}\langle\mu|\vec{\sigma}\cdot\left(\hat{\vec{p}}\,\hat{V}\times\hat{\vec{p}}\right)|\nu\rangle\\ &-\frac{\mathrm{i}}{4c^2}\langle\mu|\sqrt{\frac{Q(l_\mu)}{Z_\mu}}\left(\hat{\vec{p}}\,\hat{V}\times\hat{\vec{p}}\right)\sqrt{\frac{Q(l_\nu)}{Z_\nu}}|\nu\rangle\,,\end{aligned}\tag{A5}$$

where Z_μ denotes the nuclear charge associated with the atom center of the basis function χ_μ. $Q(l_\mu)$ is a parameter depending on the angular momentum quantum number of the basis function[113]

$$Q(l) = 0, 2, 10, 28 \qquad \text{for} \qquad l = 0, 1, 2, 3\tag{A6}$$

and for higher l quantum numbers[120]

$$Q(l \geq 4) = l(l+1)(2l+1)/3.\tag{A7}$$

Note that we apply the screening parameters directly to the integrals as suggested in ref. 177.

A formally more sophisticated ansatz is the spin–orbit mean field (SOMF) approach.[114] Here, the two-electron spin–orbit operator

$$\hat{\vec{g}}^{\mathrm{SO}}(i,j) = -\frac{1}{2c^2}r_{ij}^{-3}\left[\vec{r}_{ij}\times\hat{\vec{p}}(i)\right]\tag{A8}$$

is explicitly included. i, j denote the two electrons. This leads to the spin-same orbit (SSO) contributions of the form $\left(\hat{\vec{g}}^{\mathrm{SO}}(i,j)\cdot\hat{\vec{s}}(i)\right)$ and to the spin-other orbit (SOO) contributions of the form $2\left(\hat{\vec{g}}^{\mathrm{SO}}(j,i)\cdot\hat{\vec{s}}(j)\right)$. In SOMF, an effective one-electron operator

$$\hat{H}^{\mathrm{SOMF}} = \sum_i \hat{\vec{z}}(i)\cdot\hat{\vec{s}}(i)\tag{A9}$$

is derived. The matrix representation of the operator $\hat{\vec{z}}$ is defined as[178]

$$
\begin{aligned}
\langle\mu|\hat{\vec{z}}|\nu\rangle = \quad & \langle\mu|\hat{\vec{h}}^{\mathrm{SO}}|\nu\rangle + \sum_{\kappa\lambda} P_{\kappa\lambda}\,(\mu\nu|\hat{\vec{g}}^{\mathrm{SO}}|\kappa\lambda) \\
& - \frac{3}{2}\sum_{\kappa\lambda} P_{\kappa\lambda}\left[(\mu\kappa|\hat{\vec{g}}^{\mathrm{SO}}|\lambda\nu) + (\lambda\nu|\hat{\vec{g}}^{\mathrm{SO}}|\mu\kappa)\right].
\end{aligned}
\tag{A10}
$$

See refs. 114 and 178 for details on the derivation. Strategies for the implementation are described in ref. 115.

Within the framework of exact two-component theory, the picture-change correction is applied to the one-electron spin–orbit perturbation[52]

$$
h_{\mu\nu}^{\text{SO-X2C}} = \frac{\mathrm{i}}{4c^2}\sum_{\kappa,\lambda} U_{\mu\kappa}^{\mathrm{SL},\dagger}\,\langle\kappa|\vec{\sigma}\cdot\left(\hat{\vec{p}}\,\hat{V}\times\hat{\vec{p}}\right)|\lambda\rangle\, U_{\lambda\nu}^{\mathrm{SL}} \tag{A11}
$$

where $U_{\mu\nu}^{\mathrm{SL}}$ is a matrix element of the small-large block of the unitary decoupling transformation. The large-large block is not needed for the SO perturbation. In X2C, the matrix $\mathbf{U}$ is obtained in one step by a diagonalization of the (one-electron) Dirac matrix[63–69] and closely related to the normalized elimination of the small component (NESC).[179–183] The unitary decoupling transformation can be accelerated using the diagonal local approximation to the unitary decoupling transformation[116,117]

$$
\mathbf{U}^{\mathrm{LL}} = \bigoplus_{A}\mathbf{U}_{AA}^{\mathrm{LL}}, \tag{A12}
$$

$$
\mathbf{U}^{\mathrm{SL}} = \bigoplus_{A}\mathbf{U}_{AA}^{\mathrm{SL}}, \tag{A13}
$$

where the transformation matrix is approximated as a direct sum of so-called atomic diagonal blocks, AA, which are defined with the atom center of the basis functions. Application of the SNSO approach for the X2C spin–orbit perturbation is done analogously to eqs. A3 and A5. Two sets of parameters for the SNSO ansatz were applied to X2C, the original ones of Boettger and reoptimized ones by the group of Cremer.[118–120] The latter approach is termed modified SNSO (mSNSO). Here, the cases for the angular momentum are defined as

$$
Q'(l) = \begin{cases} Q(l) & \text{if } Z > Q(l) \\ Q(l') & \text{if } Z \leq Q(l) \end{cases} \tag{A14}
$$

with l' denoting the maximal orbital angular momentum number, l, so that $Z > Q(l')$. This improves the accuracy for virtual spinor states.[118] Further, some parameters were reoptimized with the xenon and radon atom resulting in[118]

$$
Q'(1) = 2.34\,\mathrm{erf}\,(34500/\zeta_p), \tag{A15}
$$

$$
Q'(2) = 11.0, \tag{A16}
$$

$$
Q'(3) = 28.84, \tag{A17}
$$

where ζ_p indicates the exponent of the p-type basis function. We note that other spin–orbit perturbation approaches in X2C were discussed in the literature[184–189] but not yet applied to ZFS parameters.

REFERENCES

[1] M. R. Pederson and S. N. Khanna, Phys. Rev. B **60**, 9566 (1999).
[2] H. J. F. Jansen, Phys. Rev. B **59**, 4699 (1999).
[3] S. Sinnecker and F. Neese, J. Phys. Chem. A **110**, 12267 (2006).
[4] F. Neese, J. Am. Chem. Soc. **128**, 10213 (2006).
[5] F. Neese, J. Chem. Phys. **127**, 164112 (2007).
[6] R. Takeda, S. Mitsuo, S. Yamanaka, and K. Yamaguchi, Polyhedron **24**, 2238 (2005).
[7] R. Reviakine, A. V. Arbuznikov, J.-C. Tremblay, C. Remenyi, O. L. Malkina, V. G. Malkin, and M. Kaupp, J. Chem. Phys. **125**, 054110 (2006).
[8] C. van Wüllen, J. Chem. Phys. **130**, 194109 (2009).
[9] S. Schmitt, P. Jost, and C. van Wüllen, J. Chem. Phys. **134**, 194113 (2011).
[10] E. M. V. Kessler, S. Schmitt, and C. van Wüllen, J. Chem. Phys. **139**, 184110 (2013).
[11] K. Sugisaki, K. Toyota, K. Sato, D. Shiomi, and T. Takui, J. Phys. Chem. A **120**, 9857 (2016).
[12] D. Wu, C. Zhou, J. J. Bao, L. Gagliardi, and D. G. Truhlar, J. Chem. Theory Comput. **18**, 2199 (2022).
[13] F. Neese and E. I. Solomon, Inorg. Chem. **37**, 6568 (1998).
[14] Z. Havlas and J. Michl, J. Chem. Soc., Perkin Trans. 2 , 2299 (1999).
[15] O. Vahtras, O. Loboda, B. Minaev, H. Ågren, and K. Ruud, Chem. Phys. **279**, 133 (2002).
[16] O. Loboda, B. Minaev, O. Vahtras, B. Schimmelpfennig, H. Ågren, K. Ruud, and D. Jonsson, Chem. Phys. **286**, 127 (2003).
[17] C. de Graaf and C. Sousa, Int. J. Quantum Chem. **106**, 2470 (2006).
[18] D. Ganyushin and F. Neese, J. Chem. Phys. **125**, 024103 (2006).
[19] M. Sundararajan, D. Ganyushin, S. Ye, and F. Neese, Dalton Trans. , 6021 (2009).
[20] D. Ganyushin, N. Gilka, P. R. Taylor, C. M. Marian, and F. Neese, J. Chem. Phys. **132**, 144111 (2010).
[21] K. Sugisaki, K. Toyota, K. Sato, D. Shiomi, M. Kitagawa, and T. Takui, Chem. Phys. Lett. **477**, 369 (2009).
[22] K. Sugisaki, K. Toyota, K. Sato, D. Shiomi, M. Kitagawa, and T. Takui, ChemPhysChem **11**, 3146 (2010).
[23] K. Sugisaki, K. Toyota, K. Sato, D. Shiomi, and T. Takui, Phys. Chem. Chem. Phys. **19**, 30128 (2017).
[24] T. Bodenstein, A. Heimermann, K. Fink, and C. van Wüllen, ChemPhysChem **23**, e202100648 (2022).
[25] W. Van den Heuvel and A. Soncini, J. Chem. Phys. **138**, 054113 (2013).
[26] J. Vaara, S. A. Rouf, and J. Mareš, J. Chem. Theory Comput. **11**, 4840 (2015).
[27] B. Martin and J. Autschbach, J. Chem. Phys. **142**, 054108 (2015).
[28] B. Martin and J. Autschbach, Phys. Chem. Chem. Phys. **18**, 21051 (2016).
[29] Neese, Frank, in *Calculation of NMR and EPR Parameters: Theory and Applications*, edited by M. Kaupp, M. Bühl, and V. G. Malkin (Wiley-VCH, Weinheim, Germany, 2004) Chap. 34, pp. 541–564.
[30] R. McWeeny, Y. Mizuno, and C. A. Coulson, Proc. Royal Soc. Lond. A **259**, 554 (1961).
[31] H. A. Bethe and E. E. Salpeter, *Quantum mechanics of one-and two-electron atoms* (Springer, Berlin, Heidelberg, Germany, 1957).
[32] A. E. Reed, R. B. Weinstock, and F. Weinhold, J. Chem. Phys. **83**, 735 (1985).
[33] R. A. Friesner, Chem. Phys. Lett. **116**, 39 (1985).
[34] R. A. Friesner, J. Chem. Phys. **85**, 1462 (1986).
[35] R. A. Friesner, J. Chem. Phys. **86**, 3522 (1987).
[36] F. Neese, F. Wennmohs, A. Hansen, and U. Becker, Chem. Phys. **356**, 98 (2009).
[37] R. Izsák and F. Neese, J. Chem. Phys. **135**, 144105 (2011).
[38] R. Izsák, F. Neese, and W. Klopper, J. Chem. Phys. **139**, 094111 (2013).
[39] B. Helmich-Paris, B. de Souza, F. Neese, and R. Izsák, J. Chem. Phys. **155**, 104109 (2021).
[40] P. Plessow and F. Weigend, J. Comput. Chem. **33**, 810 (2012).
[41] C. Holzer, J. Chem. Phys. **153**, 184115 (2020).
[42] H. Laqua, T. H. Thompson, J. Kussmann, and C. Ochsenfeld, J. Chem. Theory Comput. **16**, 1456 (2020).
[43] T. J. Martinez and E. A. Carter, "Pseudospectral methods applied to the electron correlation problem," in *Modern Electronic Structure Theory –*

Part II, edited by D. R. Yarkony (World Scientific Press, Singapore, 1995) Chap. 17, pp. 1132–1165.

[44] J. Jaramillo, G. E. Scuseria, and M. Ernzerhof, J. Chem. Phys. **118**, 1068 (2003).

[45] J. F. Dobson, J. Chem. Phys. **98**, 8870 (1993).

[46] A. D. Becke, J. Chem. Phys. **117**, 6935 (2002).

[47] J. Tao, Phys. Rev. B **71**, 205107 (2005).

[48] J. E. Bates and F. Furche, J. Chem. Phys. **137**, 164105 (2012).

[49] C. Holzer, Y. J. Franzke, and M. Kehry, J. Chem. Theory Comput. **17**, 2928 (2021).

[50] Y. J. Franzke, C. Holzer, and F. Mack, J. Chem. Theory Comput. **18**, 1030 (2022).

[51] Y. J. Franzke and C. Holzer, J. Chem. Phys. **157**, 031102 (2022).

[52] F. Bruder, Y. J. Franzke, and F. Weigend, J. Phys. Chem. A **126**, 5050 (2022).

[53] C. Holzer, Y. J. Franzke, and A. Pausch, J. Chem. Phys. **157**, 204102 (2022).

[54] C. J. Schattenberg and M. Kaupp, J. Chem. Theory Comput. **17**, 1469 (2021).

[55] R. Grotjahn, F. Furche, and M. Kaupp, J. Chem. Phys. **157**, 111102 (2022).

[56] A. Pausch and C. Holzer, J. Phys. Chem. Lett. **13**, 4335 (2022).

[57] Y. Zhao and D. G. Truhlar, J. Chem. Phys. **125**, 194101 (2006).

[58] Y. Zhao and D. G. Truhlar, Theor. Chem. Acc. **120**, 215 (2008).

[59] J. Sun, A. Ruzsinszky, and J. P. Perdew, Phys. Rev. Lett. **115**, 036402 (2015).

[60] J. W. Furness, A. D. Kaplan, J. Ning, J. P. Perdew, and J. Sun, J. Phys. Chem. Lett. **11**, 8208 (2020).

[61] J. W. Furness, A. D. Kaplan, J. Ning, J. P. Perdew, and J. Sun, J. Phys. Chem. Lett. **11**, 9248 (2020).

[62] M. Bursch, H. Neugebauer, S. Ehlert, and S. Grimme, J. Chem. Phys. **156**, 134105 (2022).

[63] W. Kutzelnigg and W. Liu, J. Chem. Phys. **123**, 241102 (2005).

[64] W. Liu and W. Kutzelnigg, J. Chem. Phys. **126**, 114107 (2007).

[65] W. Liu and D. Peng, J. Chem. Phys. **125**, 044102 (2006).

[66] W. Liu and D. Peng, J. Chem. Phys. **125**, 149901 (2006).

[67] M. Iliaš and T. Saue, J. Chem. Phys. **126**, 064102 (2007).

[68] W. Liu and D. Peng, J. Chem. Phys. **131**, 031104 (2009).

[69] D. Peng, W. Liu, Y. Xiao, and L. Cheng, J. Chem. Phys. **127**, 104106 (2007).

[70] P. Pyykkö, Annu. Rev. Phys. Chem. **63**, 45 (2012).

[71] T. Saue, ChemPhysChem **12**, 3077 (2011).

[72] J. Autschbach, J. Chem. Phys. **136**, 150902 (2012).

[73] W. Liu, J. Chem. Phys. **152**, 180901 (2020).

[74] D. Peng and M. Reiher, Theor. Chem. Acc. **131**, 1081 (2012).

[75] J. Autschbach, "Relativistic effects on magnetic resonance parameters and other properties of inorganic molecules and metal complexes," in *Relativistic Methods for Chemists*, edited by M. Barysz and Y. Ishikawa (Springer Netherlands, Dordrecht, 2010) pp. 521–598.

[76] J. Autschbach, Philos. Trans. A Math. Phys. Eng. Sci. **372**, 20120489 (2014).

[77] K. G. Dyall and K. Fægri Jr., *Introduction to Relativistic Quantum Chemistry* (Oxford University Press, New York, NY, USA, 2007).

[78] M. Reiher and A. Wolf., *Relativistic Quantum Chemistry – The Fundamental Theory of Molecular Science*, 2nd ed. (Wiley-VCH, Weinheim, Germany, 2015).

[79] W. Liu, ed., *Handbook of Relativistic Quantum Chemistry* (Springer, Berlin, Heidelberg, Germany, 2017).

[80] M. M. Roessler and E. Salvadori, Chem. Soc. Rev. **47**, 2534 (2018).

[81] M. Kaupp, M. Bühl, and V. G. Malkin, eds., *Calculation of NMR and EPR Parameters. Theory and Applications* (Wiley-VCH, Weinheim, Germany, 2004).

[82] F. Neese, "Quantum Chemistry and EPR Parameters," in *eMagRes*, Vol. 6, edited by R. K. Harris and R. L. Wasylishen (John Wiley & Sons, Chichester, United Kingdom, 2017) pp. 1–22.

[83] D. Goldfarb and S. Stoll, eds., *EPR Spectroscopy: Fundamentals and Methods* (John Wiley & Sons, Chichester, United Kingdom, 2018).

[84] J. R. Cheeseman, G. W. Trucks, T. A. Keith, and M. J. Frisch, J. Chem. Phys. **104**, 5497 (1996).

[85] J. Autschbach, S. Patchkovskii, and B. Pritchard, J. Chem. Theory Comput. **7**, 2175 (2011).

[86] G. Vignale and M. Rasolt, Phys. Rev. Lett. **59**, 2360 (1987).

[87] E. R. Johnson, J. Chem. Phys. **141**, 124120 (2014).

[88] C. Holzer and Y. J. Franzke, J. Chem. Phys. **157**, 034108 (2022).

[89] T. M. Maier, A. V. Arbuznikov, and M. Kaupp, WIREs Comput. Mol. Sci. **9**, e1378 (2018).

[90] A. V. Arbuznikov and M. Kaupp, J. Chem. Phys. **136**, 014111 (2012).

[91] J. Tao, V. N. Staroverov, G. E. Scuseria, and J. P. Perdew, Phys. Rev. A **77**, 012509 (2008).

[92] A. V. Arbuznikov and M. Kaupp, J. Chem. Phys. **141**, 204101 (2014).

[93] T. M. Maier, M. Haasler, A. V. Arbuznikov, and M. Kaupp, Phys. Chem. Chem. Phys. **18**, 21133 (2016).

[94] H. Bahmann and M. Kaupp, J. Chem. Theory Comput. **11**, 1540 (2015).

[95] C. J. Schattenberg, K. Reiter, F. Weigend, and M. Kaupp, J. Chem. Theory Comput. **16**, 931 (2020).

[96] M. Häser, R. Ahlrichs, H. P. Baron, P. Weis, and H. Horn, Theor. Chim. Acta **83**, 455 (1992).

[97] K. Reiter, F. Mack, and F. Weigend, J. Chem.Theory Comput. **14**, 191 (2018).

[98] Y. J. Franzke and F. Weigend, J. Chem. Theory Comput. **15**, 1028 (2019).

[99] S. Gillhuber, Y. J. Franzke, and F. Weigend, J. Phys. Chem. A **125**, 9707 (2021).

[100] Y. J. Franzke and J. M. Yu, J. Chem. Theory Comput. **18**, 323 (2022).

[101] Y. J. Franzke and J. M. Yu, J. Chem. Theory Comput. **18**, 2246 (2022).

[102] Y. J. Franzke and C. Holzer, ChemRxiv (2023), 10.26434/chemrxiv-2023-k8jwn-v3.

[103] R. Ahlrichs, M. Bär, M. Häser, H. Horn, and C. Kölmel, Chem. Phys. Lett. **162**, 165 (1989).

[104] S. G. Balasubramani, G. P. Chen, S. Coriani, M. Diedenhofen, M. S. Frank, Y. J. Franzke, F. Furche, R. Grotjahn, M. E. Harding, C. Hättig, A. Hellweg, B. Helmich-Paris, C. Holzer, U. Huniar, M. Kaupp, A. Marefat Khah, S. Karbalaei Khani, T. Müller, F. Mack, B. D. Nguyen, S. M. Parker, E. Perlt, D. Rappoport, K. Reiter, S. Roy, M. Rückert, G. Schmitz, M. Sierka, E. Tapavicza, D. P. Tew, C. van Wüllen, V. K. Voora, F. Weigend, A. Wodyński, and J. M. Yu, J. Chem. Phys. **152**, 184107 (2020).

[105] Y. J. Franzke, C. Holzer, J. H. Andersen, T. Begušié, F. Bruder, S. Coriani, F. Della Sala, E. Fabiano, D. A. Fedotov, S. Fürst, S. Gillhuber, R. Grotjahn, M. Kaupp, M. Kehry, M. Krstié, F. Mack, S. Majumdar, B. D. Nguyen, S. M. Parker, F. Pauly, A. Pausch, E. Perlt, G. S. Phun, A. Rajabi, D. Rappoport, B. Samal, T. Schrader, M. Sharma, E. Tapavicza, R. S. Treß, V. Voora, A. Wodyński, J. M. Yu, B. Zerulla, F. Furche, C. Hättig, M. Sierka, D. P. Tew, and F. Weigend, J. Chem. Theory Comput. (2023), 10.1021/acs.jctc.3c00347.

[106] TURBOMOLE GmbH, (2023), developers' version of TURBOMOLE V7.7.1, a development of University of Karlsruhe and Forschungszentrum Karlsruhe GmbH, 1989-2007, TURBOMOLE GmbH, since 2007; available from `https://www.turbomole.org` (retrieved July 26, 2023).

[107] F. Mack, C. J. Schattenberg, M. Kaupp, and F. Weigend, J. Phys. Chem. A **124**, 8529 (2020).

[108] O. Treutler, *Entwicklung und Anwendung von Dichtefunktionalmethoden*, Dissertation (Dr. rer. nat.), University of Karlsruhe (TH), Germany (1995).

[109] O. Treutler and R. Ahlrichs, J. Chem. Phys. **102**, 346 (1995).

[110] Y. J. Franzke, R. Treß, T. M. Pazdera, and F. Weigend, Phys. Chem. Chem. Phys. **21**, 16658 (2019).

[111] S. Koseki, M. W. Schmidt, and M. S. Gordon, J. Phys. Chem. **96**, 10768 (1992).

[112] S. G. Chiodo and M. Leopoldini, Comput. Phys. Commun. **185**, 676 (2014).

[113] J. C. Boettger, Phys. Rev. B **62**, 7809 (2000).

[114] B. A. Heß, C. M. Marian, U. Wahlgren, and O. Gropen, Chem. Phys. Lett. **251**, 365 (1996).

[115] B. Helmich-Paris, C. Hättig, and C. van Wüllen, J. Chem. Theory Comput. **12**, 1892 (2016).

[116] D. Peng and M. Reiher, J. Chem. Phys. **136**, 244108 (2012).

[117] D. Peng, N. Middendorf, F. Weigend, and M. Reiher, J. Chem. Phys. **138**, 184105 (2013).

[118] M. Filatov, W. Zou, and D. Cremer, J. Chem. Phys. **139**, 014106 (2013).

[119] W. Zou, M. Filatov, and D. Cremer, J. Chem. Phys. **142**, 214106 (2015).

[120] T. Yoshizawa, W. Zou, and D. Cremer, J. Chem. Phys. **145**, 184104 (2016).

[121] M. Kehry, Y. J. Franzke, C. Holzer, and W. Klopper, Mol. Phys. **118**, e1755064 (2020).

[122] Y. J. Franzke, N. Middendorf, and F. Weigend, J. Chem. Phys. **148**, 104410 (2018).

[123] Y. J. Franzke, F. Mack, and F. Weigend, J. Chem. Theory Comput. **17**, 3974 (2021).

[124] Y. J. Franzke, J. Chem. Theory Comput. **19**, 2010 (2023).

[125] M. Balmer, Y. J. Franzke, F. Weigend, and C. von Hänisch, Chem. Eur. J. **26**, 192 (2020).

[126] T. M. Maier, H. Bahmann, and M. Kaupp, J. Chem. Theory Comput. **11**, 4226 (2015).

[127] U. Ekström, L. Visscher, R. Bast, A. J. Thorvaldsen, and K. Ruud, J. Chem. Theory Comput. **6**, 1971 (2010).

[128] M. A. L. Marques, M. J. T. Oliveira, and T. Burnus, Comput. Phys. Commun. **183**, 2272 (2012).

[129] S. Lehtola, C. Steigemann, M. J. T. Oliveira, and M. A. L. Marques, SoftwareX **7**, 1 (2018).

[130] "Libxc," Version 6.2.2, available from `https://www.tddft.org/programs/libxc/` (retrieved July 26, 2023).

[131] A. Klamt and G. Schüürmann, J. Chem. Soc., Perkin Trans. 2 , 799 (1993).

[132] A. Schäfer, A. Klamt, D. Sattel, J. C. W. Lohrenz, and F. Eckert, Phys. Chem. Chem. Phys. **2**, 2187 (2000).

[133] OpenMP Architecture Review Boards, "OpenMP API shared-memory parallel programming," `https://www.openmp.org` (retrieved August 15, 2023).

[134] C. Holzer and Y. J. Franzke, OpenMP version of ridft, rdgrad, and egrad with contributions to mpshift, dscf, and grad; improved OpenMP version of aoforce and escf, released with TURBOMOLE V7.4 and further improved in TURBOMOLE V7.5, see `https://www.turbomole.org/turbomole/release-notes-turbomole-7-5/` (retrieved July 31, 2023).

[135] K. P. Huber and G. H. Herzberg, *Constants of Diatomic Molecules* (Van Nostrand Reinhold, New York, NY, USA, 1979) see also `https://webbook.nist.gov/` (retrieved August 1, 2023).

[136] F. Neese, WIREs Comput. Mol. Sci. **12**, e1606 (2022).

[137] F. Neese, "ORCA – an ab initio, density functional and semiempirical program package, V. 5.0.4, MPI für Kohlenforschung, Mülheim a. d. Ruhr (Germany)," (2023).

[138] A. D. Becke, Phys. Rev. A **38**, 3098 (1988).

[139] J. P. Perdew, Phys. Rev. B **33**, 8822 (1986).

[140] J. P. Perdew, K. Burke, and M. Ernzerhof, Phys. Rev. Lett. **77**, 3865 (1996).

[141] C. Adamo and V. Barone, J. Chem. Phys. **110**, 6158 (1999).

[142] F. Weigend and R. Ahlrichs, Phys. Chem. Chem. Phys. **7**, 3297 (2005).

[143] F. Weigend, Phys. Chem. Chem. Phys. **8**, 1057 (2006).

[144] J.-N. Rebilly, G. Charron, E. Rivière, R. Guillot, A.-L. Barra, M. D. Serrano, J. van Slageren, and T. Mallah, Chem. Eur. J. **14**, 1169 (2008).

[145] S. Ye, F. Neese, A. Ozarowski, D. Smirnov, J. Krzystek, J. Telser, J.-H. Liao, C.-H. Hung, W.-C. Chu, Y.-F. Tsai, R.-C. Wang, K.-Y. Chen, and H.-F. Hsu, Inorg. Chem. **49**, 977 (2010).

[146] C. Lee, W. Yang, and R. G. Parr, Phys. Rev. B **37**, 785 (1988).

[147] A. D. Becke, J. Chem. Phys. **98**, 1372 (1993).

[148] J.-D. Chai and M. Head-Gordon, Phys. Chem. Chem. Phys. **10**, 6615 (2008).

[149] N. Mardirossian and M. Head-Gordon, J. Chem. Phys. **142**, 074111 (2015).

[150] N. Mardirossian and M. Head-Gordon, J. Chem. Phys. **144**, 214110 (2016).

[151] J. Tao, J. P. Perdew, V. N. Staroverov, and G. E. Scuseria, Phys. Rev. Lett. **91**, 146401 (2003).

[152] V. N. Staroverov, G. E. Scuseria, J. Tao, and J. P. Perdew, J. Chem. Phys. **119**, 12129 (2003).

[153] S. Grimme, J. Phys. Chem. A **109**, 3067 (2005).

[154] M. Haasler, T. M. Maier, R. Grotjahn, S. Gückel, A. V. Arbuznikov, and M. Kaupp, J. Chem. Theory Comput. **16**, 5645 (2020).

[155] P. Pollak and F. Weigend, J. Chem. Theory Comput. **13**, 3696 (2017).

[156] R. Ahlrichs and K. May, Phys. Chem. Chem. Phys. **2**, 943 (2000).

[157] Y. J. Franzke, L. Spiske, P. Pollak, and F. Weigend, J. Chem. Theory Comput. **16**, 5658 (2020).

[158] V. S. Mironov, T. A. Bazhenova, Y. V. Manakin, K. A. Lyssenko, A. D. Talantsev, and E. B. Yagubskii, Dalton Trans. **46**, 14083 (2017).

[159] F. J. Birk, D. Pinkowicz, and K. R. Dunbar, Angew. Chem. Int. Ed. **55**, 11368 (2016).

[160] K. S. Pedersen, M. Sigrist, M. A. Sørensen, A.-L. Barra, T. Weyhermüller, S. Piligkos, C. A. Thuesen, M. G. Vinum, H. Mutka, H. Weihe, R. Clérac, and J. Bendix, Angew. Chem. Int. Ed. **53**, 1351 (2014).

[161] T. D. Harris, M. V. Bennett, R. Clérac, and J. R. Long, J. Am. Chem. Soc. **132**, 3980 (2010).

[162] J. Martínez-Lillo, T. F. Mastropietro, E. Lhotel, C. Paulsen, J. Cano, G. De Munno, J. Faus, F. Lloret, M. Julve, S. Nellutla, and J. Krzystek, J. Am. Chem. Soc. **135**, 13737 (2013).

[163] E. Caldeweyher, S. Ehlert, A. Hansen, H. Neugebauer, S. Spicher, C. Bannwarth, and S. Grimme, J. Chem. Phys. **150**, 154122 (2019).

[164] D. Andrae, U. Häußermann, M. Dolg, H. Stoll, and H. Preuß, Theor. Chim. Acta **77**, 123 (1990).

[165] TURBOMOLE GmbH, (2023), manual of TURBOMOLE V7.7.1, a development of University of Karlsruhe and Forschungszentrum Karlsruhe GmbH, 1989-2007, TURBOMOLE GmbH, since 2007; available from `https://www.turbomole.org/turbomole/turbomole-documentation/` (retrieved July 26, 2023).

[166] S. Lehtola, M. Dimitrova, H. Fliegl, and D. Sundholm, J. Chem. Theory Comput. **17**, 1457 (2021).

[167] S. Lehtola, M. Dimitrova, H. Fliegl, and D. Sundholm, J. Chem. Theory Comput. **17**, 4629 (2021).

[168] S. Lehtola and M. A. L. Marques, J. Chem. Phys. **157**, 174114 (2022).

[169] A. Kubica, J. Kowalewski, D. Kruk, and M. Odelius, J. Chem. Phys. **138**, 064304 (2013).

[170] M. Atanasov, D. Aravena, E. Suturina, E. Bill, D. Maganas, and F. Neese, Coord. Chem. Rev. **289-290**, 177 (2015).

[171] W. Nakanishi, S. Hayashi, Y. Katsura, and M. Hada, J. Phys. Chem. A **115**, 8721 (2011).

[172] T. B. Demissie, J. Chem. Phys. **147**, 174301 (2017).

[173] A. Wodyński and M. Kaupp, J. Phys. Chem. A **123**, 5660 (2019).

[174] M. Douglas and N. M. Kroll, Ann. Phys. (NY) **82**, 89 (1974).

[175] B. A. Hess, Phys. Rev. A **33**, 3742 (1986).

[176] G. Jansen and B. A. Hess, Phys. Rev. A **39**, 6016 (1989).

[177] C. van Wüllen and C. Michauk, J. Chem. Phys. **123**, 204113 (2005).

[178] F. Neese, J. Chem. Phys. **122**, 034107 (2005).

[179] K. G. Dyall, J. Chem. Phys. **106**, 9618 (1997).

[180] K. G. Dyall, J. Chem. Phys. **109**, 4201 (1998).

[181] K. G. Dyall and T. Enevoldsen, J. Chem. Phys. **111**, 10000 (1999).

[182] K. G. Dyall, J. Chem. Phys. **115**, 9136 (2001).

[183] D. Cremer, W. Zou, and M. Filatov, WIREs Comput. Mol. Sci. **4**, 436 (2014).

[184] Z. Li, Y. Xiao, and W. Liu, J. Chem. Phys. **137**, 154114 (2012).

[185] Z. Li, Y. Xiao, and W. Liu, J. Chem. Phys. **141**, 054111 (2014).

[186] L. Cheng and J. Gauss, J. Chem. Phys. **141**, 164107 (2014).

[187] B. Mussard and S. Sharma, J. Chem. Theory Comput. **14**, 154 (2018).

[188] L. Cheng, F. Wang, J. F. Stanton, and J. Gauss, J. Chem. Phys. **148**, 044108 (2018).

[189] C. Zhang and L. Cheng, Mol. Phys. **118**, e1768313 (2020).